MECHANISTIC DETAILS OF THE PH-DEPENDENT ASSOCIATION OF BOTULINUM NEUROTOXIN WITH MEMBRANES

By

Darren J. Mushrush

Dissertation

Submitted to the Faculty of the

Graduate School of Vanderbilt University

in partial fulfillment of the requirements

for the degree of

DOCTOR OF PHILOSOPHY

in

Biochemistry

December, 2011

Nashville, Tennessee

Approved:

D. Borden Lacy

Hassane S. Mchaourab

Michael R. Waterman

Charles R. Sanders

Richard N. Armstrong

ACKNOWLEDGEMENTS

I would like thank first and foremost Dr. Borden Lacy. I began my scientific journeys with Borden as a research assistant and she supported my plans to return to my graduate studies and pursue a PhD under her guidance. I deeply appreciate her scientific insight, guidance, allowing me to be stubborn, listening to my crazy schemes, and keeping a level head when I could not.

I would also like to extend my gratitude to all my colloborators, Dr. Mauricio Montal, Dr. Audrey Fischer, Dr. Hassane Mchaourab and Dr. Hanane A. Koteiche. We began our collaboration with Hassane, who also served on my dissertation committee, while I was still a research assistant and he has always been eager to help. He has offered his personnel, equipment, and advice. His energy and enthusiasm for knowledge is amazing and this project couldn't have been done without him. Special thanks must go to Hanane who helped me collect and analyze almost all my EPR data by giving up large parts of her week. She was the main person that helped me develop my EPR methodology and a listener to my ideas. Hanane was there for all the disappointing data collection days and shared the excitement when we saw something new and intriguing.

I want to thank Dr. Michael Waterman who has been involved in my scientific training since I began as a graduate student both as a mentor and as a friend. He has supported me in all my scientific endeavors and has imparted a lot of life wisdom that will not be forgotten.

I want to thank all of the remaining members of my dissertation committee, Dr. Richard Armstrong and Dr. Charles Sanders, for providing me with experimental expertise and their continued support in my pursuit of a PhD.

I want to thank the Lacy Lab members, new and old, for creating an enjoyable lab environment, for not breaking the FPLC too often, and for allowing me to be myself.

These studies were supported by the NIH (RO1AI075259).

TABLE OF CONTENTS

LIST OF TABLES

Table

LIST OF FIGURES

LIST OF ABBREVIATIONS

BoNT	Botulinum Neurotoxin
EM	Electron Microscopy
EPR	Electron Paramagnetic Resonance
ESI	Electrospray Ionization
HC	Heavy Chain
HCT	Translocation Domain
HCR	Receptor-binding Domain
IANBD	*N*-((2-(iodoacetoxy)ethyl)- *N*-methyl)amino-7-nitrobenz-2-oxa-1,3-diazole
LC	Light Chain
LUV	Large Unilamellar Vesicles
MTSSL	*S*-(2,2,5,5-tetramethyl-2,5-dihydro-1H-pyrrol-3-yl)methyl methanethiosulfonate
PFT	Pore-forming Toxin
PL	Proteoliposome
POPC	1-palmitoyl-2-oleoyl-*sn*-glycero-3-phosphocholine
POPG	1-palmitoyl-2-oleoyl-*sn*-glycero-3-phospho-(1'-rac-glycerol)
SNAP-25	Soluble NSF Attachment Protein 25
Syt	Synaptotagmin

CHAPTER I

INTRODUCTION

Clostridium botulinum

Clostridium botulinum is a rod shaped, obligate anaerobe that is capable of forming spores and is commonly found in soil. It is most notable for the production of the potent neurotoxin, botulinum neurotoxin or BoNT, the causative agent of botulism. The disease and etiology of botulism was first defined by van Ermengen in 1895 during an outbreak from salted raw ham in Ellezelles, Belgium. van Ermengen concluded that "it is highly probable that the poison in the ham was produced by anaerobic growth of specific microorganisms during the salting process" [1, 2] He also concluded that the disease was from an intoxication rather than an infection [1, 2]. The organism was first defined as *Bacillus botulinus* but was later reclassified due to the restriction of the *Bacillus* genus to aerobes.

Clostridium botulinum classification

The heterogeneous species *C. botulinum* is comprised of phylogenetically and physiologically diverse bacteria and is defined by the capacity of these bacteria to produce botulinum neurotoxin (BoNT). Strains of *C. botulinum* are traditionally categorized into seven serological types (A through G) [3]. These seven serological types have been classified into four metabolic types and also contain *C. butyricum and C. baratii*, which produce a toxin that cross-reacts with type E and F, respectively [4-6].

They have been divided into *C. botulinum* groups I-IV and are genetically different enough to merit four different species that are, in fact, more divergent than *B. subtilis* and *Staphylococcus aureus* [7] (Table 1).

Proteolytic strains have a clostridial protease that results in post-translational proteolysis of the toxin [8]. Proteolytic strains (Group I and IV) include toxins A, B, F, and G. These strains can produce a single active toxin (e.g. type A), can contain genes for two toxins but only produce a single toxin (e.g type A(B) which contains genes for both A and B serotypes but only produces A), or can contain genes for two toxins and produce one as a major and one as a minor toxin (e.g. type Ab, which would produce more type A serotype than type B) [9]. Non-proteolytic strains (Groups II and III) include serotypes B, E, and F and produce only a single active toxin. In either of these strain classifications, the toxin gene can be located on the bacterial chromosome or on a large plasmid [10].

Botulism

Botulism is a rare, yet potentially deadly disease caused by exposure to BoNT. Exposure occurs through 3 major pathways: foodborne intoxication, wound infection, and intestinal colonization. The clinical syndrome involves symmetrical cranial nerve palsies followed by descending symmetric flaccid paralysis of the voluntary muscles that can lead to respiratory failure [11, 12]. Botulism should be diagnosed and treated with anti-toxin in less than 24 hours from the onset of symptoms. The anti-toxin only neutralizes toxin that is not bound to or has not entered nerve endings. Once inside the nerve cell

Table 1. Phenotypic differences between botulinum neurotoxin producing organisms.

Characteristic	Groups					
	I	II	III	IV	*C. butyricum*	*C. baratii*
Serotype	A,B,F	B,E,F	C,D	G	E	F
Proteolysis	+	-	-	+	-	-

there is no treatment to prevent disease. Severe intoxication may require intubation due to paralysis of the diaphragm and accessory breathing muscles. Untreated botulism results in death due to the airway obstruction from pharyngeal muscle paralysis and a decrease in lung volume due to diaphragm and breathing muscle paralysis [11].

Foodborne botulism results from ingestion of food that has been contaminated with the toxin and does not require the bacteria to be present. It is most commonly associated with two food sources. One is in non-acidic canned foods, such as asparagus or mushrooms, where improper heating during the canning process has occurred. Home-canned foods are a major source of intoxication in the United States [13]. The other is native foods where the food is generally fermented and eaten uncooked [11]. This provides a suitable environment for spore germination. Between 1990 and 2000 there were 263 botulism cases in the United States resulting from foodborne events [14].

Wound botulism results from an infection at an open wound. *C. botulinum* spores can get into an open wound and germinate in the anaerobic conditions of an abscess. The conditions allow for *in situ* production of the toxin which can then access the blood stream in an intestine-independent manner. While historically rare, the incidence of wound botulism in the United States has increased dramatically with the increase in needle-drug use [15]. Almost all of the needle-associated wound botulism comes from the use of "black tar heroin" [16].

Intestinal botulism results from the germination of *C. botulinum* within the intestines of infants or adults. Infants less than year of age are particularly susceptible due to an 'immature' normal intestinal flora that is less able to prevent *C. botulinum* germination and growth. Infant botulism is the most common form of botulism and

results in between 80 to 100 cases a year in the United States [13]. Honey is a known source of *C. botulinum* spores and has been implicated in about 20% of all infant botulism cases [17, 18]. Adult intestinal toxemia results from a similar colonization of the intestine with *C. botulinum* and is typically a result of deformations within the bowel or extended antimicrobial therapy [19-21].

Inhalation botulism is not a naturally occurring intoxication but can occur through the aerosol dissemination of BoNT [22, 23]. Inhalation intoxication poses a security risk due to the potential for weaponization of BoNT and the lack of a preventative vaccine.

BoNT Function

BoNT belongs to a class of proteins known as AB toxins. These toxins have an A fragment containing catalytic activity and a B fragment that delivers the A fragment into the cell cytosol. Once the A fragment is released into the cytosol it can target its specific host protein (Figure 1). A number of very potent toxins, including anthrax toxin, diphtheria toxin, and cholera toxin, belong to the AB toxin class.

BoNT acts at the neuromuscular junction to block the release of acetylcholine vesicles into the synapse. BoNT binds the neuron and is taken into the cell by receptor-mediated endocytosis. The pH drop in the endosome results in conformational changes that support membrane insertion of the B fragment and subsequent translocation of the A fragment into the cell cytosol. Once the A fragment is within the cytosol it can cleave proteins involved in synaptic vesicle fusion.

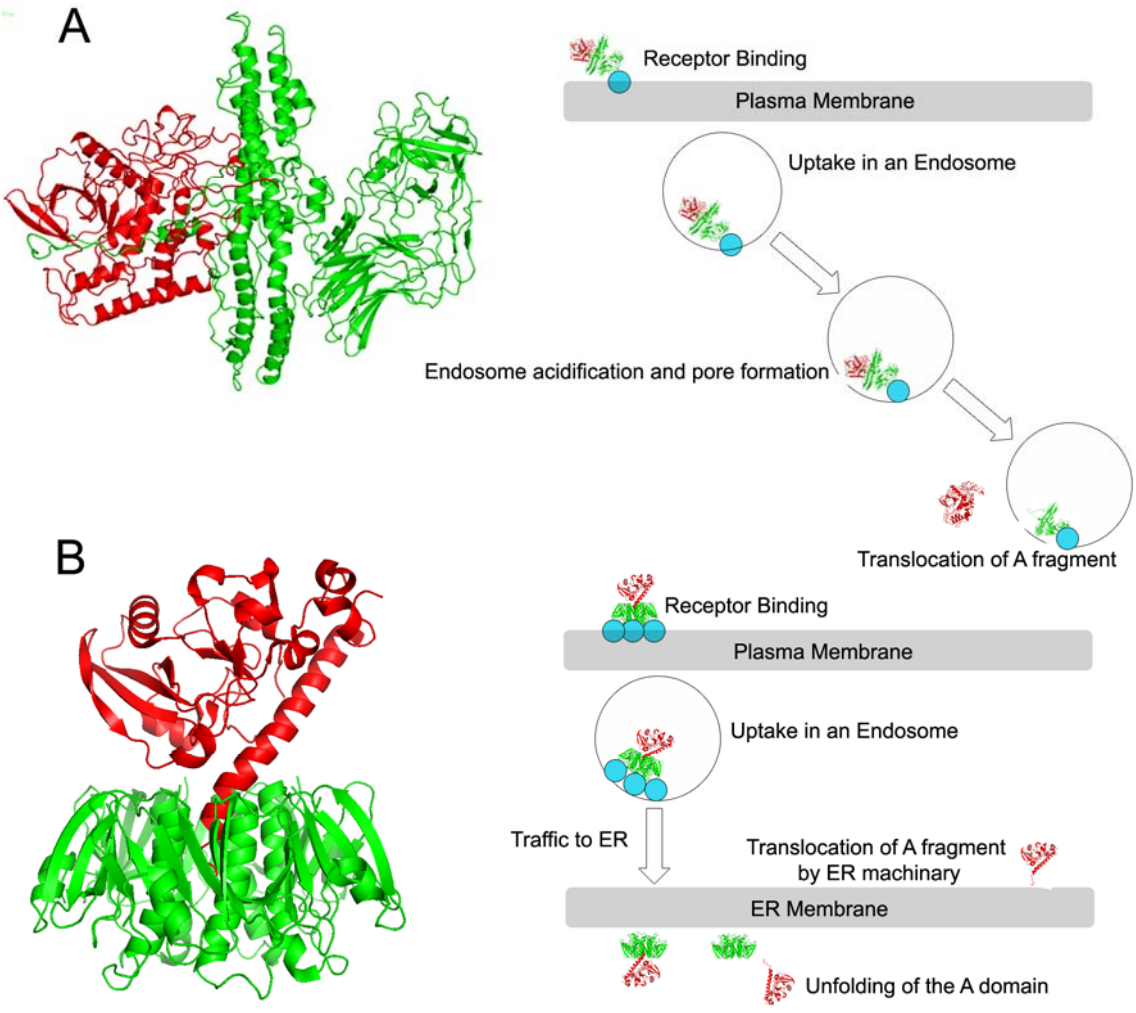

Figure 1. AB toxin pathways of entry. A) Example pathway using BoNT, an AB toxin. B fragment (green) of BoNT binds to a surface receptor and is taken up using receptor mediated endocytosis. The maturation and acidification of the endosome results in pore formation by the B fragment which allows for translocation of the A fragment (red) into the endosome. B) Example pathway using cholera toxin, an AB5 toxin. B fragment (green) binds to a surface receptor and oligomerizes. Receptor-mediated endocytosis traffics the toxin to the ER. The A fragment (red) is unfolded and translocated into the cystol by ER machinery and refolds [24].

Botulinum Neurotoxin Structure

BoNT is expressed as a single 150 kDa polypeptide chain. Proteolytic strains cleave, or 'nick', the polypeptide chain into a more toxic dichain form using a clostridial protease while non-proteolytic strains are believed to rely on a gut protease to generate the dichain form. Generation of the dichain form leaves a 50 kDa light chain (LC) and a 100 kDa heavy chain (HC) that remain tethered together by a disulfide bond (Figure 2A). The LC is composed of a single zinc endoprotease domain. The HC is made up of two distinct domains, each about 50 kDa in size (Figure 2B). The translocation domain is located at the N-terminus of the HC and is abbreviated HCT. This domain forms a pore within the membrane of acidified endosomes and delivers the LC into the cytosol of the target host cell. The receptor-binding domain is located at the C-terminus of the HC and is abbreviated HCR. This domain is responsible for binding specific receptors at the neuromuscular junction and results in receptor-mediated endocytosis of the toxin.

The crystal structure for the BoNT holotoxin has been determined using BoNT/A (PDB 3BTA) [25, 26], BoNT/B (PDB 1EPW) [27], and BoNT/E (PDB 3FFZ) [28]. The crystal structures are notable in that they reveal an elongated translocation domain with a 50 amino acid 'belt' that wraps around the LC. The crystal structures of BoNT/A and /B have a linear arrangement of the three domains with the LC and HCR separated by the HCT. BoNT/E has the HCR rotated 180^{o} to lie adjacent to the LC, a configuration that has been observed in both the crystal structure and single particle reconstruction [28, 29].

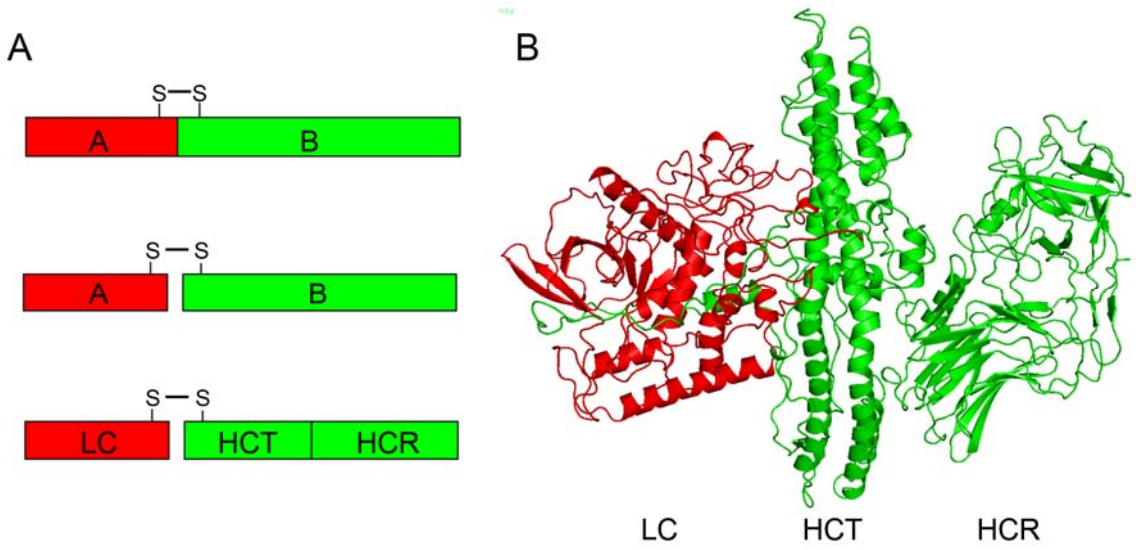

Figure 2. AB organization of BoNT Structure. A) BoNT is produced as single polypeptide AB toxin that is proteolytically cleaved to separate the A fragment from the B fragment. The two chains remained tethered by a disulfide bond. The A fragment consisted of the 50 kDa LC. The B fragment consists of the 50 kDa HCT and the 50 kDa HCR. B) Crystal structure of BoNT/A showing the modular domain organization.

Receptor-Binding Domain (HCR)

HCR is a two-lobed domain composed of two distinct subdomains (HCR_N and HCR_C) joined by an α-helix (Figure 3). It is predominantly made up of β-strand secondary structure with distinct motifs for each subdomain. The HCR_N adopts a jelly-roll motif from two seven stranded β–sheets, whereas the HCR_C adopts a modified β–trefoil and β–barrel fold [27, 28, 30]. Despite being adjacent to the HCT in sequence, the HCR makes minimal structural contact with the HCT domain.

The interaction of BoNT with the neuronal membrane is thought to require two receptors; a general receptor in the form of ganglioside and a high affinity protein receptor that confers serotype specificity [31, 32]. The ganglioside(s) that bind each serotype have been defined [33-38]. BoNT serotypes A, B, C, and F bind G_{T1b}, G_{D1b}, and G_{D1a} [34-36, 38, 39]. BoNT/E binds G_{T1b} and G_{D1a} [33, 35] whereas BoNT/G recognizes all gangliosides with equal affinity [35]. BoNT/D lacks a ganglioside binding pocket but binds phosphatidylethanolamine (PE). Blocking the ability of BoNT to bind ganglioside is protective [35, 40]. The first protein receptor identified was the vesicle fusion protein synaptotagmin (Syt) [41, 42], which is recognized by BoNT/B [43-45]. BoNT/G, like BoNT/B, binds both SytI and SytII isoforms [46]. Crystal structures of the complex between BoNT/B and an α-helical SytII peptide reveal the details of the binding site within HCR_C [47-50] (Figure 3).

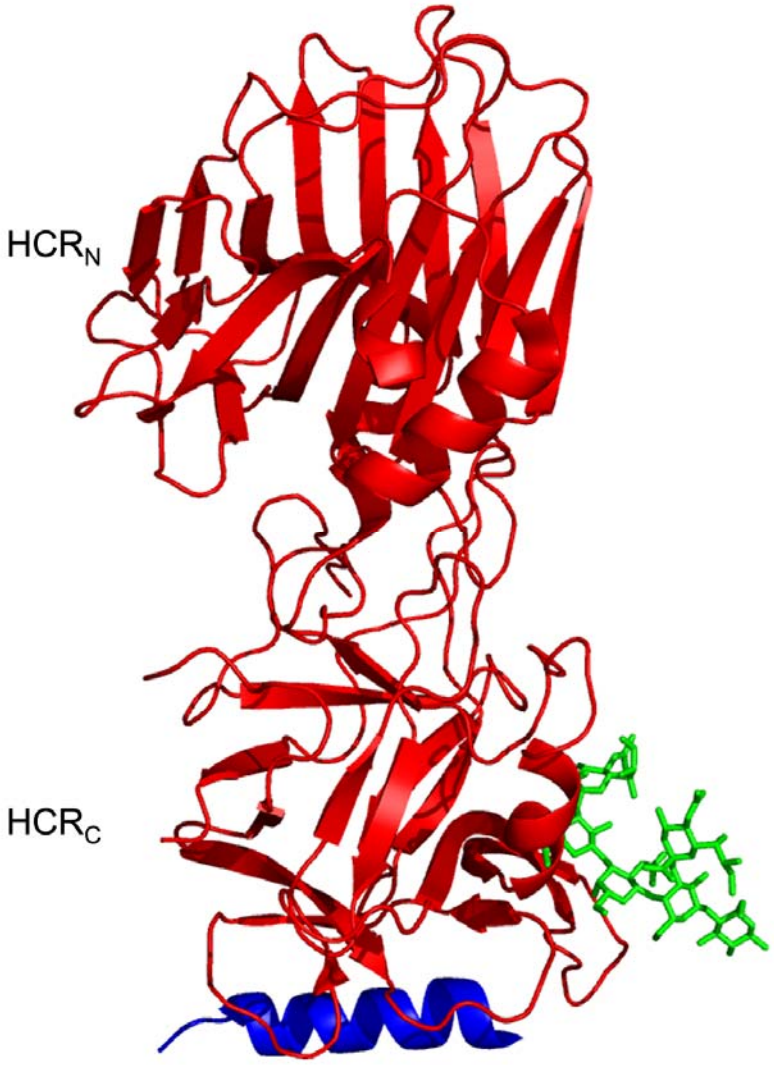

Figure 3. BoNT/B HCR bound to Syt II (2NM1). Crystal structure of BoNT/B HCR (red) in complex with Syt II (blue). G_{T1b} (green) docked into the ganglioside binding site was superimposed from a structure of BoNT/A HCR in complex with G_{T1b} (2VU9). Both receptors bind the C-terminal lobe of the HCR (HCR_C).

SV2 is an integral membrane glycoprotein with 12 putative transmembrane spanning regions that acts as the receptor for BoNT/A (SV2) [51], BoNT/E (glycosylated SV2A and SV2B) [52], BoNT/F (glycosylated SV2) [53], and more recently BoNT/D (SV2) [54]. Although no crystal structure has been determined of any SV2 isoform with any BoNT serotype, it is believed that a 130 amino acid extracellular loop is the site of binding for BoNT/A and BoNT/E [51, 52]. It has not yet been established where BoNT/F or BoNT/D interact, though it is known that they require both ganglioside and SV2 binding for neuronal uptake [53, 54]. BoNT/C has had no protein receptor identified and is believed to only bind ganglioside as a neuronal receptor [39, 55, 56].

Catalytic Domain (LC)

The catalytic domain (or LC) is a zinc metalloprotease that cleaves synaptic fusion SNARE (SNAP Receptor) proteins in order to inhibit vesicle/membrane fusion. It is a globular structure composed of both α-helical and β-sheet secondary structure (Figure 2B). The domain is surrounded by a 50 amino acid 'belt' from the translocation domain that partially occludes the active site [25, 27, 28]. The LC remains tethered to the HCT after nicking through a disulfide bond between residues C429 of the LC and C453 of the HCT domain [25, 27] (Figure 2A). The low pH within the mature endosomes is thought to cause unfolding of the LC. Once inside the cytosol the LC refolds into a functional zinc endopeptidase specific for one of the three SNARE proteins. Serotypes A, C and E cleave SNAP25 located at the plasma membrane [57-62]. Serotypes B, D, F, and G cleave VAMP/Synaptobrevin which is located on the synaptic vesicle [57, 63-67].

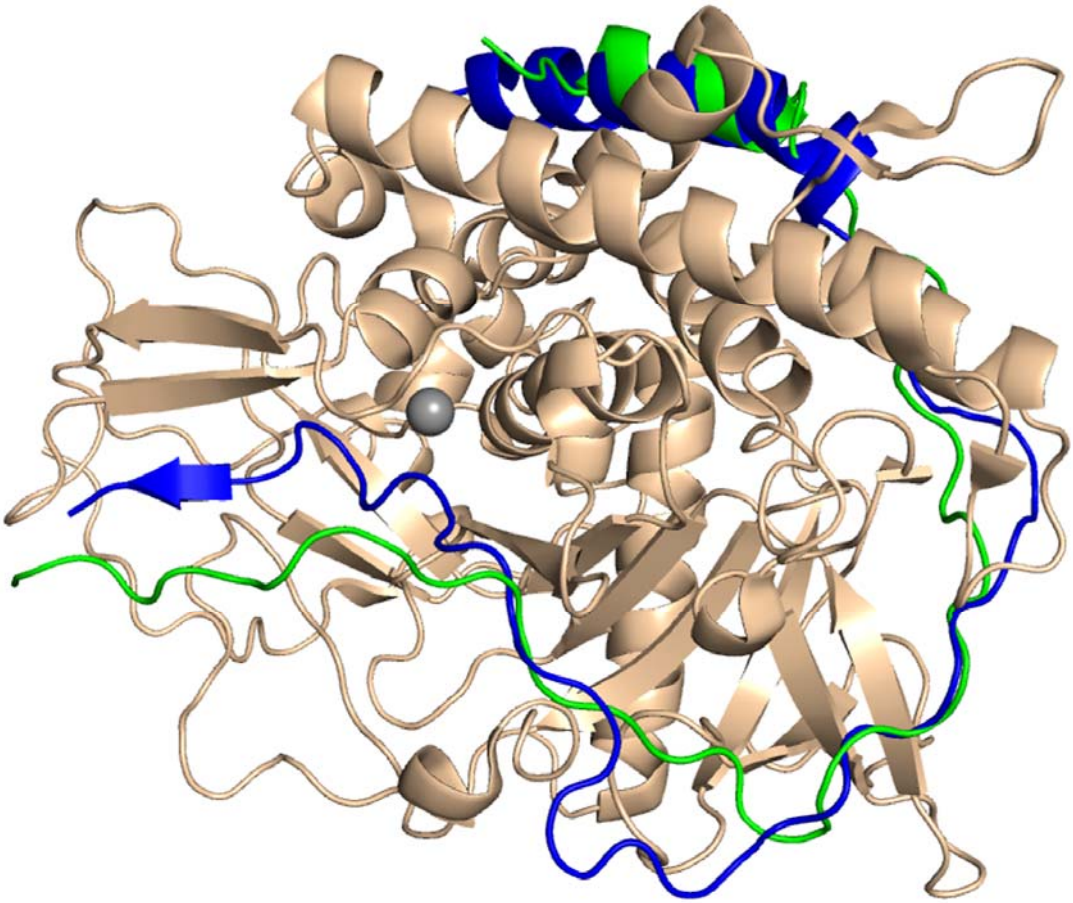

Figure 4. BoNT/A LC complexed with SNAP-25. Cocrystal structure of BoNT/A LC (wheat) bound to a SNAP-25 (blue). SNAP-25 makes extensive contacts with the LC outside the active site. The wrapping of SNAP-25 around the LC domain resembles the structure of the HCT belt (green) in the structure of the holotoxin (3BTA). The active site zinc is depicted as the grey sphere.

Serotype C also cleaves Syntaxin, which is located at the plasma membrane [68, 69]. The cleavage site is specific for each serotype. Structural analysis of BoNT/A LC bound to a peptide of SNAP-25 shows extensive interaction between the two molecules [70, 71]. The peptide wraps around the LC in a similar manner as the HCT belt (Figure 4). The LC contains two exosites to accommodate the larger peptide and orient the scissile bond toward the zinc for cleavage [70].

Translocation Domain (HCT)

HCT, the domain involved in pore formation and LC translocation, is a predominantly α-helical structure with a few unique features (Figure 5). The N-terminal half of the domain (residues 453-688) is comprised predominantly of loops with a few short α–helices interspersed and includes the cysteine (C453) involved in the disulfide linkage with the LC and a 50 amino acid 'belt' that wraps around the LC [25, 27, 28]. The belt occupies a similar position as the substrate and covers a large part of the LC surface utilized for substrate binding yet contains no scissile bond [70, 72]. The binding to substrate exosites may help the LC to refold into a catalytically functional state after translocation by providing scaffolding which would be similar to a competent binding state [72]. The C-terminal half (689-871) is comprised of a pair of coiled-coil helices that are 105Å long. The structure of HCT has no structural similarity with any other pore-forming toxins (PFTs) (Figure 6) [73, 74].

PFTs are loosely grouped into two categories based on elements of secondary structure. α-PFTs are predicted to form channels using α-helices while β-PFTs tend to

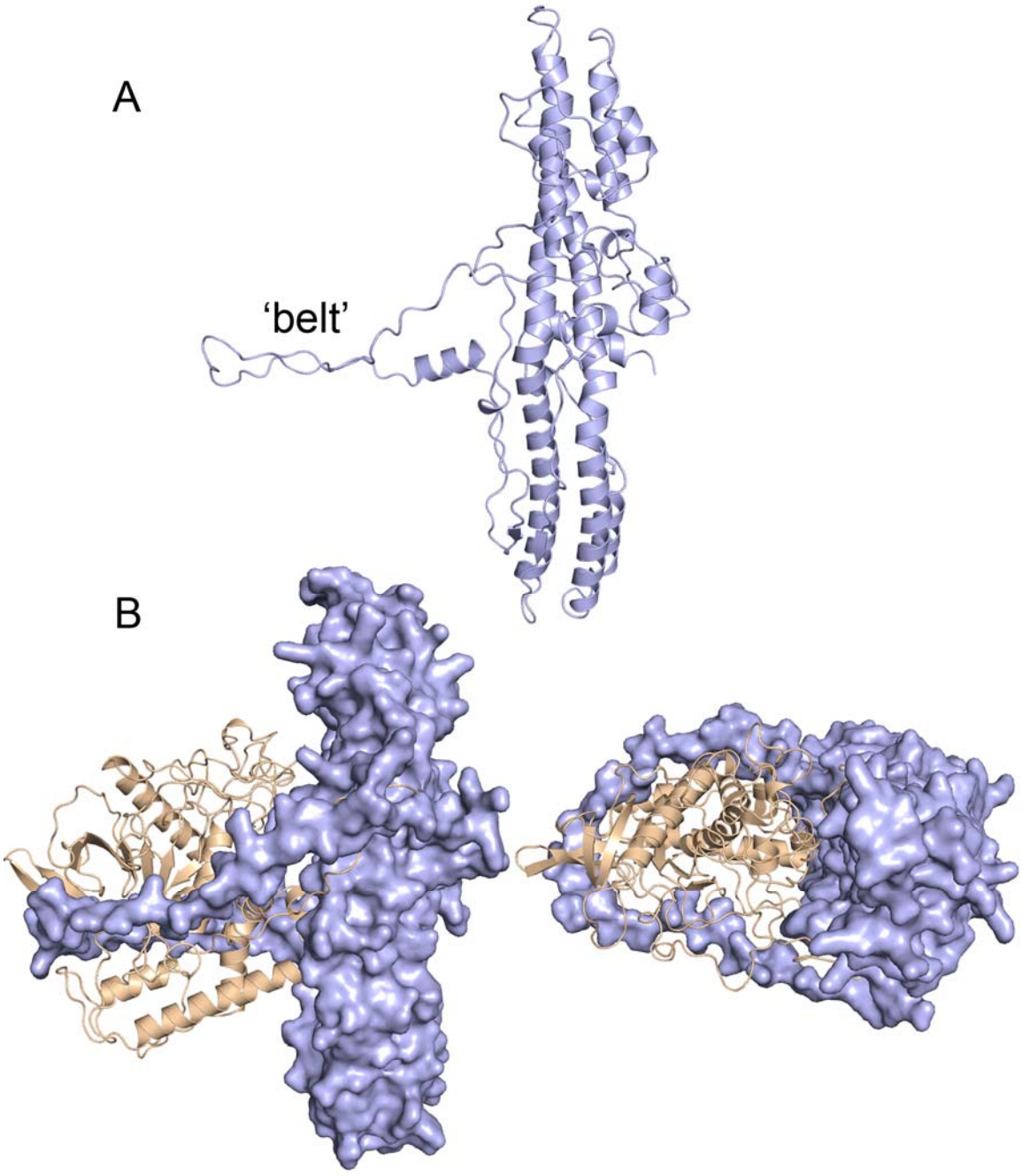

Figure 5. Structure of HCT. A) Structure of HCT domain from the holotoxin structure 3BTA. HCT is predominantly α-helical with a 50 amino acid 'belt' that extends around the LC. B) Surface representation of HCT (blue) with the LC (wheat) to highlight the 'belt'. The top view shows the 'belt' completely surrounds the LC and makes extensive contacts with the LC.

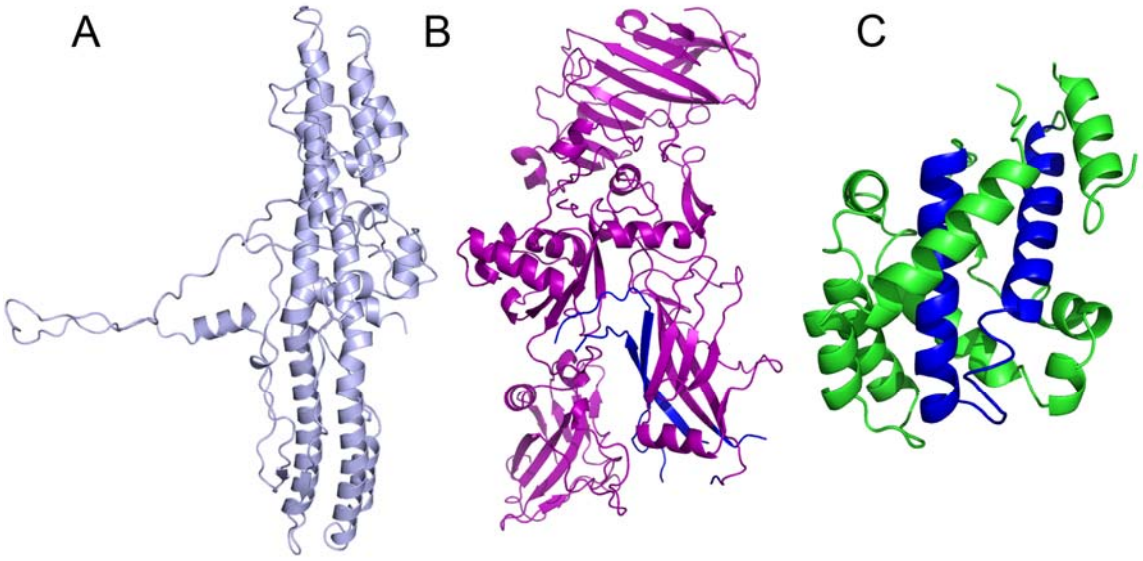

Figure 6. Crystal structures of pore forming toxins. A) Crystal structure of BoNT/A HCT, B) Crystal structure of anthrax toxin protective antigen (PA) which make a β-pore (1ACC), and C) Crystal structure of diphtheria toxin translocation domain which inserts as an α-helix (1DDT). Pore forming regions are colored dark blue for PA and diphtheria toxin. There are is no structural homology between the 3 structures despite their ability to form protein-translocating pores.

be rich in β-sheet and utilize one or two β-hairpins from each monomer to form a β-barrel structure that inserts into the membrane [75]. The rearrangement of secondary structure elements upon membrane insertion has been observed in a number of pore-forming toxins [76, 77]. For example, the insertion sequence from perfringolysin O is α-helical in the soluble protein but forms 2 transmembrane β-hairpins when inserted [76]. Knowing the secondary structure elements that span the membrane can help us understand how the resulting pore might function to transport ions, water, and/or protein.

There has been extensive work establishing BoNT as a functional pore capable of translocating the LC. The formation of ion conducting channels by BoNT has been demonstrated through the use of lipid bilayer experiments and more recently through the use of single channel clamp studies [78-83]. Translocation assays that track the movement of the LC across an artificial bilayer have shown that ion-conduction and LC translocation are connected [80, 84-87]. BoNT, and more importantly HCT, is capable of generating a protein-conducting channel that can translocate a functional LC in the absence of any host cellular proteins. Since the functions of pore-formation and translocation are isolated to HCT, understanding the unique features of the HCT should provide insight into a key mechanistic step in BoNT intoxication.

Research objectives

The goal of this research has been to understand the structures and structural changes associated with BoNT pore formation. Herein, I will describe the expression, reconstitution, and biophysical analysis of BoNT/A LC-HCT with membranes. In

collaboration with Dr. Audrey Fischer and Dr. Mauricio Montal, we have shown that LC-HCT has the same channel activity as holotoxin and can translocate LC as a functional domain (Chapter II). I have developed a liposome reconstitution system that shows association of LC-HCT with liposomes in a pH dependent manner (Chapter II). I have identified a region that is protected from pepsin when associated with liposomes and demonstrate this region moves to a more hydrophobic environment upon association with liposomes using single cysteine substitution and the cysteine-reactive environmentally-sensitive nitrobenzoxadiazole (NBD) fluorophore (Chapter III). Finally, in collaboration with Dr. Hassane Mchaourab and Dr. Hanane A. Koteiche, I performed an extensive analysis of LC-HCT single residue environments in both the soluble and liposome associated states using site-directed spin labeling and electron paramagnetic resonance spectroscopy. The analysis reveals major conformational changes in the HCT structure upon association with liposomes and indicates the formation of an oligomeric membrane-associated intermediate (Chapter IV). Together, these data support a model of how BoNT orients and associates with membranes of the endosome in response to low pH.

CHAPTER II

RECONSTITUTION IN MEMBRANES

Introduction

The BoNT intoxication mechanism involves the formation of pH-dependent pores that serve as the conduit for translocation of the LC into the cytosol. Pore formation has been localized to the HCT domain and the channels have been characterized as small and cation selective [29, 79]. The translocation of LC through these pores has been demonstrated using planar lipid bilayer and patch clamp methods and has provided significant insight into the biophysical process of pH- and potential- mediated channel activity [29, 85, 86]. The molecular structures that support pore formation and translocation have not been defined, however. This chapter summarizes our efforts to generate functional reagents for the studies that will be presented in chapters 3 and 4.

BoNT is considered a select agent, and recombinant protein expression is limited to one or two of the three functional domains. HCT is the domain associated with pore formation, but the expression of HCT alone or as HCT-HCR requires detergent solublization. Detergents pose a potential problem when assessing the pH-dependent insertion of protein into liposomes. The other 2-domain variant, LC-HCT, was likely to express as a soluble and correctly folded recombinant protein, however. Further, the presence of the LC domain would provide an enzymatic activity allowing one to assess whether translocation across a barrier occurs [84, 86]. The goals in this study were to

generate an LC-HCT protein, assess whether LC-HCT behaves similarly to holotoxin in assays of pore formation and translocation, and mimic the endosomal conditions required for membrane insertion using liposomes.

Methods

Construction of BoNT/A LC-HCT. DNA corresponding to the BoNT/A LC and HCT domains was obtained from two separate starting vectors: BoNT/A LC (unpublished results; a wild-type BoNT/A LC sequence) and HCT-SDmut [30]; a wild-type BoNT/A HCT amino acid sequence with silent mutations to disrupt an internal Shine Dalgarno site). The LC was amplified with primers that introduced a 5′ NdeI site (**GGAATTCCATATGCCATTTGTTAATAAAC**) and 3′ Sac1 site (**GGCGAGCTCGCTTATTGTATCCTTTATCTAATG**) and ligated into a TOPO vector (Invitrogen, Carlsbad, CA). An internal SacI site was then removed by *QuikChange* (Stratagene, La Jolla, CA) mutagenesis using the primer **CTCTGGCACACGAACTGATCCACGCTGGTC** and its reverse complement. The BoNT/A HCT was amplified with primers that introduced a 5′ SacI site (**GCCGAGCTCTGAACGATCTGTGTATCAAAGTTAATAATTGGG**) and 3′ XhoI site (**CCGCTCGAGGTTCTTAATATATTCAGTAAATGTAG**) and ligated into a TOPO vector. The LC and HCT domains were excised from the TOPO vectors using NdeI/SacI and SacI/XhoI, respectively and ligated into a pET24b vector that had been digested with NdeI/XhoI. The use of the engineered SacI site results in the insertion of

an Arg between K447 (cat) and A448 (trans), a feature that was included in the design to improve the efficiency of trypsin activation.

Recombinant LC-HCT Expression and Purification. The plasmid pBL031 encoding the BoNT/A LC-HCT (residues 1-870 with a C-terminal deca-His-tag, [29]) was transformed into *E. coli* BL21 DE3 (RIL) cells. A 100 ml overnight culture was added to 1 L of Terrific Broth and grown for 75 minutes. The culture was diluted two-fold into fresh media and induced using 1 mM isopropyl-β-D-thiogalactopyranoside. Cells were harvested after overnight growth at 18°C and stored at -80°C. Pellets were resuspended in 20 mM Tris-HCl pH 8.0, 150 mM NaCl and lysed using a French Press. Supernatants were clarified by centrifugation at 20,000 x g for 25 minutes and filtered with a 0.45 μm syringe disc filter. Supernatant was added to a 10 ml bed volume of Talon Metal Affinity Resin (Clontech) charged with Co^{2+}. The column was washed with 50 ml 20 mM Tris-HCl pH 8.0, 150 mM NaCl followed by 50 ml 20 mM Tris-HCl pH 8.0, 150 mM NaCl, 10 mM Imidazole. The LC-HCT protein was eluted in 20 ml 20 mM Tris-HCl pH 8.0, 150 mM NaCl, 200 mM Imidazole, concentrated to 5 ml, and purified on a Fast Flow Q Sepharose column (G.E. Healthcare) using an elution buffer gradient of 20 mM Tris-HCl pH 8.0 from 0 to 500 mM NaCl. The peak from the Q Sepharose column was concentrated to 1 ml and run over a Superdex S200 preparative grade size exclusion column (G.E. Healthcare) in 20 mM Tris-HCl 8.0, 150 mM NaCl for final purification. The retention volume was consistent with the size of a monomer based on the retention profiles of gel filtration standards (Biorad).

Construction of Single Cysteine Mutants. We mutated the 3 free cysteines (C134, C166, C790) from the wild type LC-HCT construct (pBL031) to alanines to create a LC-HCT

3CA template (plasmid pBL242). pBL242 was used as the background for all single cysteine mutations. All mutations were made using a standard *QuikChange* Site-Directed mutagenesis protocol (Stratagene) and verified by sequencing. Mutant proteins were expressed and purified as described above.

Liposome Preparation. A 2:1 mole ratio mixture of 1-palmitoyl-2-oleoyl-*sn*-glycero-3-phosphocholine:1-palmitoyl-2-oleoyl-*sn*-glycero-3-phospho-(1'-rac-glycerol) (POPC:POPG) (Avanti) in chloroform was dried under N_2 and placed under vacuum for 6 hours. The dried lipid mixture was rehydrated overnight with constant stirring to a final lipid concentration of 13 mM in 10 mM HEPES, 100 mM KCl pH 7.5. Rehydrated lipids were subjected to 3 rounds of freeze/thaw followed by extrusion through a 100 nm filter to obtain large unilamellar vesicles (LUVs).

Association and Proteoliposome Isolation. 10 μg LC-HCT (10 mg/ml) was added to 100 μl POPC/POPG in 1 ml 20 mM NaAcetate pH 4.4, 100 mM NaCl. Proteoliposomes were isolated by spinning at 10,000 x g for 10 minutes at room temperature. The supernatant was removed, and the proteoliposomes were resuspended in 1 ml 20 mM NaAcetate pH 4.4, 100 mM NaCl and then reisolated by centrifugation. This step was repeated 4 times to wash away unbound or loosely bound protein. The high pH association was performed as described above with two changes: the buffer was 20 mM Tris-HCl 8.0, 100 mM NaCl and liposomes were isolated at 100,000 x g for 45 minutes.

Trypsin Nicking of LC-HCT. Di-chain BoNT/A LC-HCT was generated by cleavage with trypsin: BoNT/A LC-HCT (0.5 mg/ml) was incubated with 1 μg/ml trypsin overnight at 22±2°C. Thereafter, trypsin was inactivated with 0.25 mg/ml trypsin soybean inhibitor for 15 min at 22±2°C.

Potassium release from POPC:POPG liposomes. Liposomes were prepared as described above. The liposomes were exchanged into 10 mM HEPES pH 7.5, 100 mM NaCl using 15 mL Sephadex G-50 size exclusion resin (Sigma). One ml of exchanged liposomes were added to 5 ml 20mM NaAcetate pH 4.8, 100 mM NaCl for low pH, 20mM NaCitrate pH 6.0, 100 mM NaCl for intermediate pH, and 10mM HEPES pH 7.0 100 mM NaCl for high pH. Using a Orion 97-19 *ionplus* Potassium Electrode (Thermo), the solution was monitored until a baseline was established. 100 µl of 10 mg/ml LC-HCT was added and the voltage was monitored. Once the voltage plateaued 5 µl of 20 mg/ml gramicidin in MeOH was added to see how much unreleased K^+ was present.

Protease activity of BoNT/A proteins. Protease activity experiments were carried out by Audrey Fischer as previously described [29]. In brief, recombinant SNAP-25 was incubated with BoNT/A holotoxin or LC-HCT and cleavage products were visualized by SDS-PAGE.

Cell culture and patch clamp recordings. Cell culture and patch clamp recordings were carried out by Audrey Fischer as previously described [29]. In brief, patches from Neuro 2A cells were excised in the inside-out configuration, and current recordings were obtained under voltage clamp conditions.

Single-channel data analysis. Data from single-channel experiments were analyzed by Audrey Fischer as previously described [29]. In brief, analysis was performed on single bursts of each experimental record. Only single bursts were analyzed due to the random duration of quiescent periods. A single burst is defined as a set of openings and closings lasting ≥50 ms bounded by quiescent periods of ≥50 ms before and after.

Cell-based intoxication assay. Cell-based intoxication assays were carried out by Audrey Fischer as previously described [29]. In brief, cleavage of endogenous SNAP-25 within Neuro 2A cells exposed to BoNT/A and truncation proteins were investigated.

Western blot analysis. Western blots were performed by Audrey Fischer as previously described [29]. In brief, whole-cell extracts were probed for the presence of SNAP-25 with anti-SNAP-25 mouse monoclonal IgG_1 and visualized using an HRP-conjugated secondary antibody.

Electron Microscopy. To visualize the association of LC-HCT with liposomes at low pH, proteoliposome pellets were analyzed by electron microscopy (EM) using conventional negative staining as described (152). Proteoliposomes were diluted to final protein concentrations of 25 to 100 μg/ml and 2.5 μl aliquots were spotted onto glow-discharged copper-mesh grids (EMS) for approximately 1 min. The grids were washed in 5 drops of 20 mM NaAcetate, pH 4.4, 100 mM NaCl followed by one drop of 0.7% uranyl formate. Grids were then incubated on one drop of 0.7% uranyl formate for 1 min, blotted against filter paper and allowed to air dry. Images of liposomes alone or proteoliposomes were recorded using a FEI Morgagni run at 100 kV at a magnification of 36,000X.

Results and Discussion

Cloning, Expression and Purification of LC-HCT.

LC-HCT was cloned by Dr. Borden Lacy into pET24b. The normal hexa-His tag was modified to a deca-His tag for purification. LC-HCT was expressed recombinantly in *E. coli* BL21 DE3 (RIL) cells because the codon usage of *E. coli* differs from *C. botulinum*. LC-HCT was expressed as a soluble, 100 kDa recombinant protein and purified to >95% purity using metal-affinity, Q-sepharose, and size-exclusion chromatography. The channel activity studies required activated LC-HCT which is the separation of the LC and HCT through proteolytic cleavage. This leaves the two domains tethered together by the disulfide between C429 and C453. Activation allows for the separation of the LC once the disulfide is reduced and can be mimicked through the use of trypsin.

The generation of mutants for fluorescence and EPR studies required the mutation of 3 of the 5 native cysteines. Native cysteines C134, C166, C790 were mutated to Ala because they lie within hydrophobic regions of soluble BoNT/A based on the crystal structure. The other two cysteines, C429 and C453, formed a disulfide bond that was stable under all purification or modification conditions.

BoNT/A LC-HCT forms a protein-conducting channel that translocates LC in a pH-dependent manner.

We compared holotoxin channel formation to that of LC-HCT in a single molecule electrophysiological assay (Figure 7). Membrane patches were obtained from

Neuro2A cells and the pipet (*cis*-compartment) was filled with low pH buffer and toxin to mimic the low pH environment of the endosome [29]. BoNT/A holotoxin and LC-HCT (Figure 7C) produce channels that begin at a low conductance of ~14 pS but progressively increase to a stable value of 68 pS when recorded at -100 mV. The ramping time and intermediate conductance states are believed to represent discrete transient steps that occur during the translocation of the LC. The HC (Figure 7A) and HCT (Figure 7B) constructs show no low conductance states [80, 84, 86]. Previous studies using lipid bilayers have shown that detection of LC catalytic activity in the *trans* compartment corresponds with the maximum channel conductance [85, 86].

For BoNT holotoxin, channel formation and LC translocation are dependent on ΔpH. The BoNT must be in a low pH buffer (~ pH 5) to mimic the pH gradient across the endosomal membrane (Figure 8A, top panel). If the *cis*-compartment containing BoNT holotoxin was held at pH 6 (Figure 8A, middle trace) or pH 7 (Figure 8A, bottom trace), no channel activity or translocation was detected [84]. We found something very different with LC-HCT. LC-HCT translocation (Figure 8B, top trace) proceeded even under a modest ΔpH (6 in the *cis*- and 7 in the *trans*- compartments) (Figure 8B, middle trace). Remarkably, when the excised membrane patches were bathed in symmetric neutral pH solutions, the LC-HCT still formed channels with a 64 pS conductance, but low conductance intermediate states were not detected (Figure 8B, lower trace, and 8C, blue). Based on CD analysis the LC remains folded at pH 7 and therefore cannot go through the ~15 Å diameter of the HCT channel [80, 84]. This allows the HCT channel activity to form channels that are unperturbed by LC translocation.

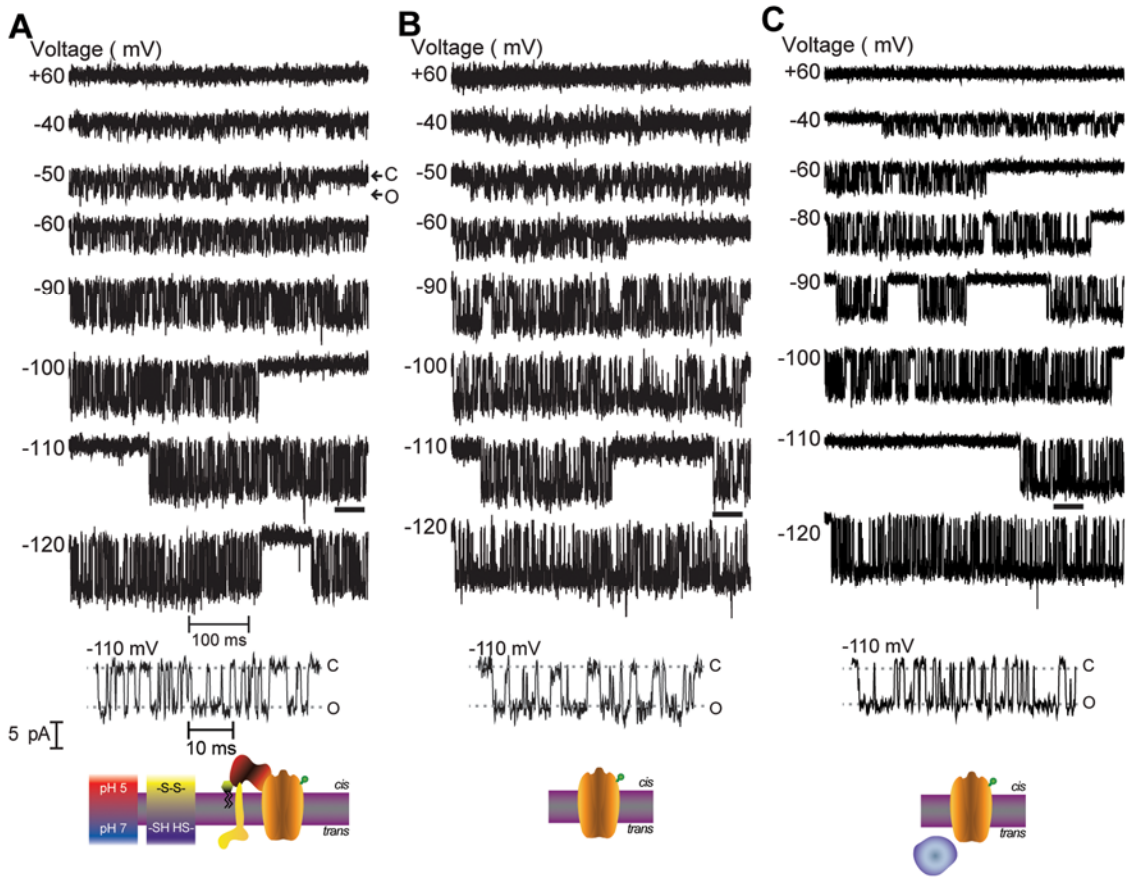

Figure 7. BoNT/A HC, HCT, and LC-HCT channel activity measured on excised patches of Neuro 2A cells. Representative single-channel currents at the indicated voltages; consecutive voltage pulses applied to the same patch for each experimental condition. Channel opening is indicated by a downward deflection; C and O denote the closed and open states. γ values for HC (A) = 65.3±0.4 pS, HCT (B) = 64.4±0.4 pS, and LC-HCT (C) = 69.2±0.9 pS. The sections of the recordings obtained at −110 mV delimited by the black bars are shown in the bottom traces at a 10-fold higher time resolution; the prototypical square events which are characteristic of unitary channel currents are clearly discerned. An interpretation of the results is schematically illustrated at the bottom of each panel: The membrane is depicted as a grey bar with magenta boundaries; LC–purple, HCT–orange, HCR–red, and the cysteine involved in the LC-HCT disulfide crosslink–green sphere; the SV2 protein-receptor is illustrated in yellow and the GT1b co-receptor in black (ceramide moiety inserted in the bilayer) and lime (the polar head group); the pH and redox conditions on the *cis* and *trans* compartments are indicated. These conventions also hold for Figure 8.

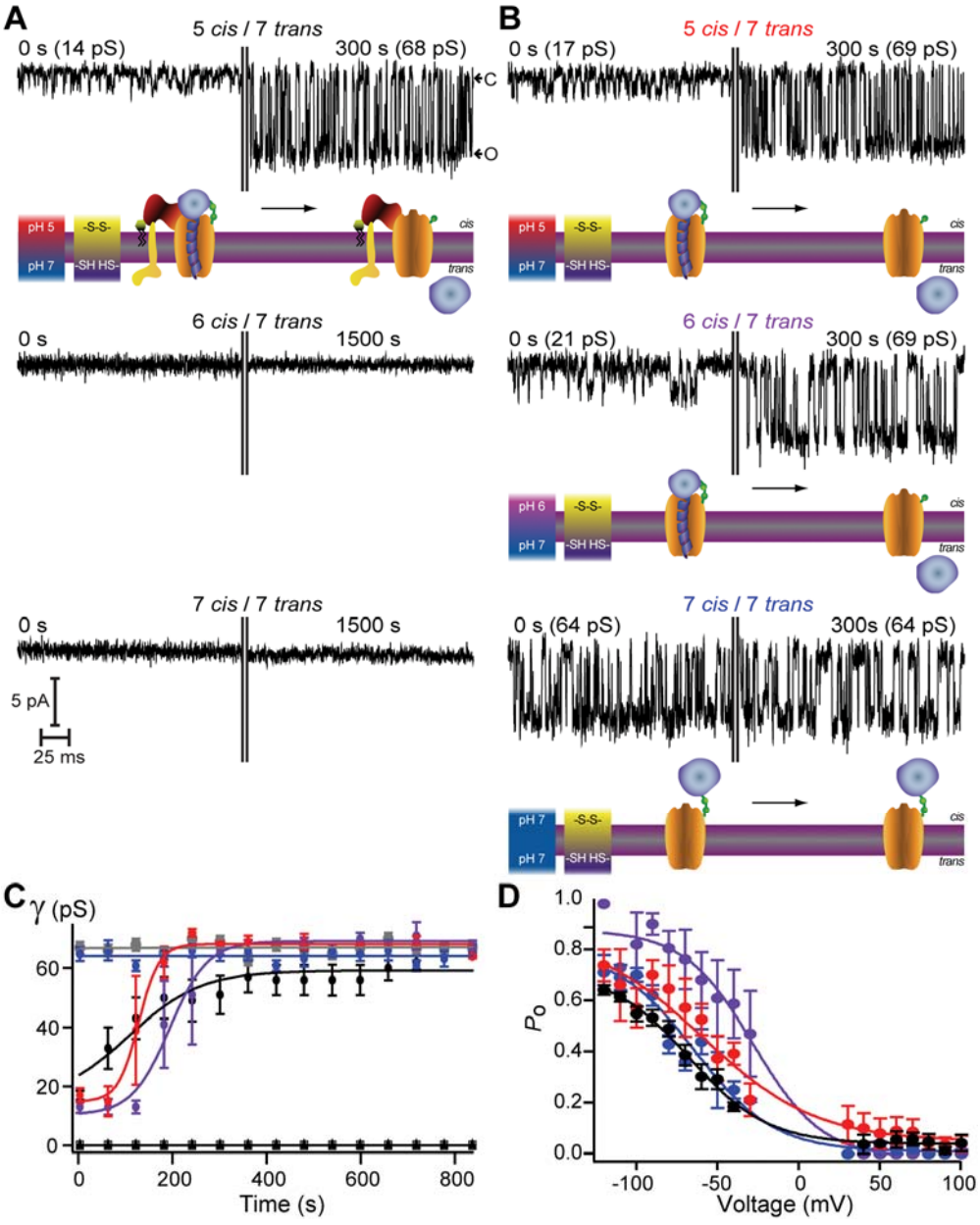

Figure 8. BoNT/A holotoxin and LC-HCT channel activity in excised patches of Neuro 2A cells over a range of pH values in the cis compartment. A and B) Top panels illustrate channel activity monitored with ΔpH 5 *cis*/7 *trans*, middle panels show ΔpH 6 *cis*/7 *trans*, and bottom panels show ΔpH, 7 *cis*/7 *trans*. (A) BoNT/A holotoxin channel activity elicited under pH 5/pH 7 begins 10 min after GΩ seal formation, t = 0 s, and transitions from a low conductance intermediate state to the unoccluded state after

completion of LC translocation. The vertical lines indicate gaps to accommodate the full recording in the limited space. A schematic representation is depicted under the records for panels A and B. BoNT/A holotoxin does not form channels under pH 6/pH 7 or pH 7/pH 7. B, BoNT/A LC-HCT channel activity begins 10 min, 12 min, and 45 min after GΩ seal formation for pH 5/pH 7, pH 6/pH 7, pH 7/pH 7, respectively. (C) Average time course of conductance change for BoNT/A holotoxin pH 5/pH 7 (black circle) ($t_{1/2}$ = 105±20 s), HC pH 5/pH 7(gray square), LC-HCT pH 5/pH 7 (red circle) ($t_{1/2}$ = 130±10 s), LC-HCT pH 6/pH 7 (magenta circle) ($t_{1/2}$ = 190±10 s), and LC-HCT pH 7/pH 7 (blue circle), ($3 \leq n \leq 6$ per data point; average N per data point = 829 events). No channel activity was detected for BoNT/A holotoxin under pH 6/pH 7 (black triangle) (n = 8) and pH 7/pH 7 (black square) (n = 8) conditions. (D) Analysis of unoccluded channel activity for BoNT/A holotoxin pH 5/pH 7 (black circle) ($V_{½}$ = −67.2±2.9 mV), BoNT/A LC-HCT for pH 5/pH 7 (red circle) ($V_{½}$ = −59.0±9.1 mV), BoNT/A LC-HCT for pH 6/pH 7 (magenta circle) ($V_{½}$ = −28.1±4.5 mV), BoNT/A LC-HCT for pH 7/pH 7 (blue circle) ($V_{½}$ = −64.1±2.9 mV).

BoNT/A LC-HCT cleaves its substrate, SNAP-25, in intact Neuro 2A cells.

The activity of LC-HCT on excised membrane patches led us to wonder whether LC-HCT would be functional on cells. BoNT/A holotoxin readily enters neuronal cells via receptor-mediated endocytosis where it then is in the proper environment for insertion and translocation. We predicted that LC-HCT would be ineffective since it lacks the HCR to provide uptake. The ability of LC-HCT to insert into the membrane and produce channels at neutral pH would suggest that insertion could occur at the plasma membrane, but we predicted that this insertion would not provide the low pH required for LC unfolding and translocation.

To test this hypothesis, we utilized a cell-based assay that monitors the amount of intact versus cleaved endogenous SNAP-25 protein within Neuro-2A cells. In the absence of BoNT/A holotoxin or in the presence of isolated HCT, SNAP-25 remained intact (Figure 9A, lanes 1 and 8), whereas in the presence of BoNT/A holotoxin, a lower molecular weight proteolysis product of ~24 kDa was detected (Figure 9A, lane 2). Surprisingly, incubation of cells with LC-HCT resulted in proteolysis of SNAP-25 (Figure 9A, lanes 3 and 4). The extent of proteolysis attained by LC-HCT was slightly lower than that produced by holotoxin but could be observed with a higher LC-HCT concentration. A single-chain BoNT/A LC-HCT unexposed to trypsin (Figure 9A, lane 5) or the LC-HCT that had the LC present in solution but released from HCT prior to the assay (Figure 9A, lane 6) did not cleave SNAP-25. Cleavage of SNAP-25 by BoNT/A LC-HCT did not occur when cells were preincubated with 2 μM bafilomycin, a vesicular proton pump inhibitor that causes the endosome to remain at a neutral pH (Figure 9A, lane 7). These results indicate that BoNT/A LC-HCT can enter neurons without the aid

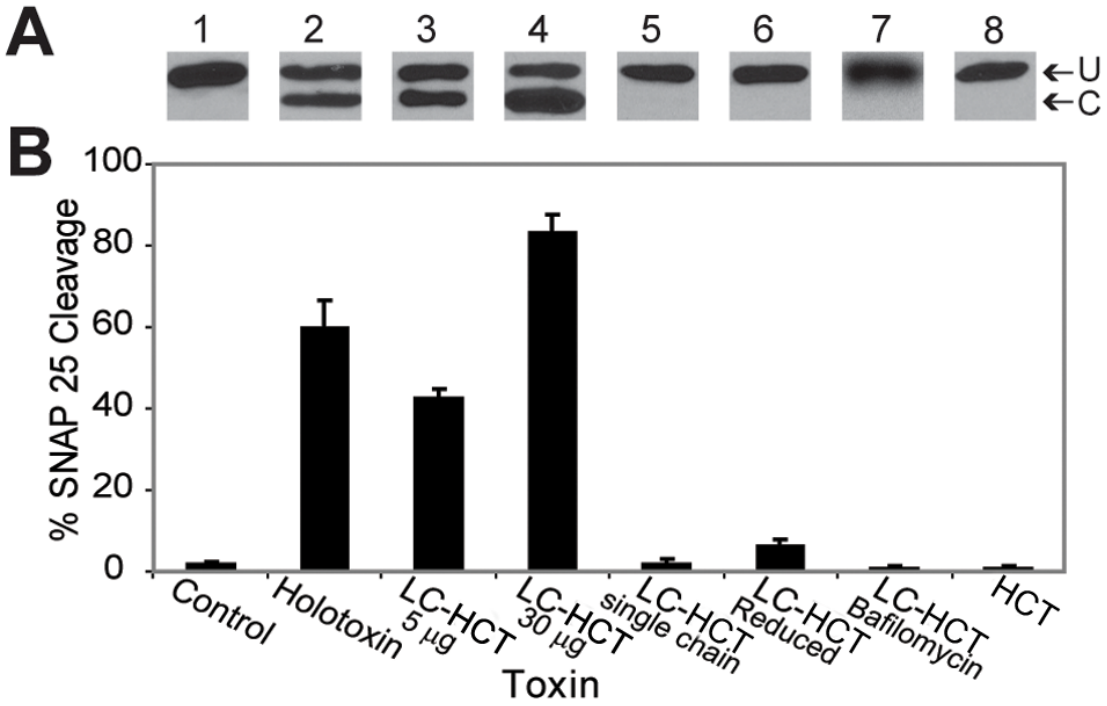

Figure 9. BoNT/A cleavage of endogenous SNAP-25 within Neuro 2A cells. (A) Representative western blot and (B) extent of SNAP-25 cleavage (average %) measured from western blots. (A) U and C denote uncleaved and cleaved SNAP-25. Blot shows SNAP-25 in the absence of BoNT/A - control (lane 1), SNAP-25 cleaved with 5 µg/well BoNT/A holotoxin (lane 2), with 5 µg/well (lane 3) and 30 µg/well (lane 4) LC-HCT. SNAP-25 was unaffected by incubation of cells with 5 µg/well BoNT/A LC-HCT single chain (lane 5) or reduced with TCEP prior to incubation with cells (lane 6), by incubation with 2 µM bafilomycin and 5 µg/well BoNT/A LC-HCT (lane 7) and by 5 µg/well BoNT/A HCT (lane 8). ($3 \leq n \leq$ per data point).

of the HCR, that LC entry does not arise from leaky cells or a non-specific mechanism, and that translocation requires the proteolytic activation step. The data were interpreted as follows: LC-HCT inserts into the plasma membrane at neutral pH and then must use a constitutive endocytic pathway to enter cells. Once inside the endosome, the low pH allows for the translocation of the LC, which can then release into the cytosol and cleave cellular SNAP-25. Together, the results provide evidence that the HCR is not necessary for channel activity or LC translocation, and that the recombinant LC-HCT is a di-modular BoNT endowed with the ability to deliver active LC protease into the cytosol of target cells.

Isolation of BoNT/A LC-HCT proteoliposomes.

Our next goal was to assess whether membrane insertion could be recapitulated in liposomes. BoNT/A LC-HCT was purified as a soluble, recombinant protein at pH 8.0. The protein was incubated at pH 4.4 or pH 8.0 in the presence or absence of POPC/POPG liposomes. While pH had no visible effect on the solubility of either protein or liposomes, the low pH incubation of the mixture resulted in aggregation, similar to what has been reported in asolectin liposomes [88]. The aggregated liposomes were isolated by centrifugation and shown to contain BoNT/A LC-HCT by SDS-PAGE. The minimal loss of LC-HCT following multiple wash and reisolation steps shows that the interaction is irreversible at low pH. The lack of LC-HCT isolated with liposomes at high pH shows that low pH is required for the LC-HCT/liposome interaction (Figure 10B). While this is in contradiction to the results obtained in the single-channel studies, we interpret this as a

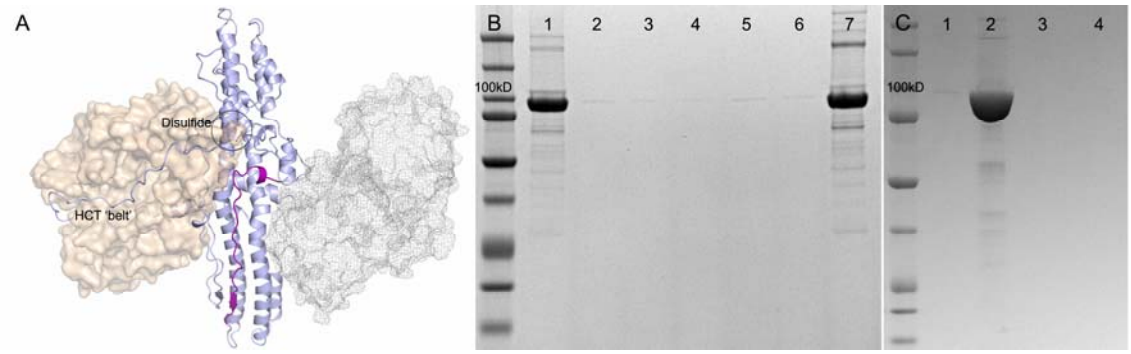

Figure 10. BoNT/A LC-HCT associates irreversibly with liposomes at low pH. A) Structure of BoNT/A. Coordinates are from model 3BTA with the HCR domain (not present in the sample) in mesh. The LC domain is shown in wheat and the HCT is shown in light blue. The disulfide and 'belt' that tether the LC and HCT structures together are highlighted to provide context of how the overall structure is arranged. The hydrophobic 659-681 sequence is colored purple. B) 10 μg LC-HCT (10 mg/ml) was added to 100 μl of POPC/POPG LUVs in 1 ml 20 mM NaAcetate pH 4.4, 100 mM NaCl. Proteoliposomes were isolated by spinning at 10,000 x g for 10 minutes at room temperature. Half of the resuspended pellet (25 μl) was reserved for analysis in Lane 1 while the remaining half was washed four times (four cycles of resuspension and centrifugation) and then analyzed in Lane 7. Supernatants from the initial proteoliposome isolation (concentrated to 50 μl) and the 4 subsequent washes (concentrated to 25 μl) were analyzed in lane 2 and lanes 3-6, respectively. C) 10 μg LC-HCT (10 mg/ml) was added to 100 μl of POPC/POPG LUVs in 1 ml 20 mM Tris-HCl 8.0, 100 mM NaCl. Liposomes were isolated at 100,000 x g for 45 minutes. Half of the resuspended pellet (25 μl) was reserved for analysis in Lane 1 and the other was resuspended in 1 ml 20 mM Tris-HCl 8.0, 100 mM NaCl and reisolated (Lane 4). The supernatants from the initial proteoliposome isolation and subsequent wash were concentrated to 25 μl and analyzed in lane 2 and lane 3, respectively. All proteins were separated by SDS-PAGE and visualized by Coomassie.

difference in now monitoring the bulk properties of the toxin. If single molecules of LC-HCT are associating with the liposomes at high pH, we will not observe them. Another important difference to note is that the channel activity assays involve an applied membrane potential, which may play a role in membrane association and insertion in the lack of a low pH environment. The liposomes, on the other hand, do not have any active generator of membrane potential.

Visualization of BoNT/A LC-HCT proteoliposomes.

The LC-HCT proteoliposomes are isolated at a centrifugation speed where free liposomes and soluble protein will not pellet. The only material we expect in the pellet are proteoliposomes, due to their aggregation, and possibly protein precipitate. We wanted to ensure that the pellet was proteoliposome, so we used negative stain EM to visualize liposomes and proteoliposomes (Figure 11). Images of free liposomes show single, round liposomes approximately 80-150 nm in diameter, consistent with the extrusion filter membrane size. Proteoliposomes show a combination of large aggregates and some single liposomes. The surfaces of the liposomes are covered in protein as seen by the staining whereas the background has minimal free LC-HCT particles. Although the organization of LC-HCT on the surface of the proteoliposome is not clear, these images provide confidence that the 10k x g pellet consists of proteoliposome and not precipitated protein.

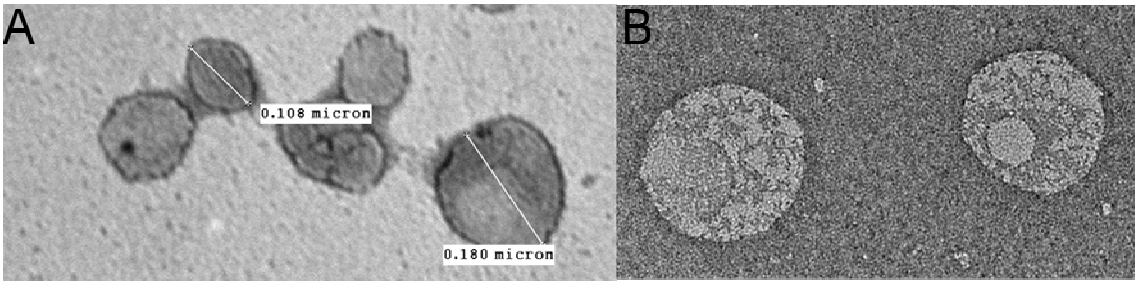

Figure 11. EM images of LC-HCT proteoliposomes. Negative stain images of liposomes alone (left) or proteoliposomes (right) were recorded using a FEI Morgagni run at 100 kV at a magnification of 36,000X. A) Liposomes without LC-HCT added. Liposome size is approximately 100-150 nm as determined by the extrusion filter. B) Proteoliposomes isolated from low pH liposome incubation with LC-HCT. The protein stains white in color from the negative stain and can be seen covering the liposome surface although no details regarding structure can be determined.

Summary

We expressed a two-domain variant of BoNT/A containing the LC and HCT. We show that the LC-HCT is a soluble protein with a channel activity similar to that observed with BoNT holotoxin. The one notable difference is that in the absence of the HCR, the LC-HCT does not have the same pH threshold requirement. We show that BoNT LC-HCT has the capacity to enter Neuro2A cells and translocate a functional LC. We have used this LC-HCT protein to develop a liposome reconstitution system that allows irreversible association of LC-HCT with liposomes under pH conditions observed in the endosome. The association of LC-HCT with liposomes can be visualized using negative stain EM.

CHAPTER III

IDENTIFICATION OF AN LC-HCT SEQUENCE THAT INTERACTS WITH LIPOSOMES

Introduction

The pore formed by BoNT in membranes is solely attributed to the HCT [29] but the sequence that inserts into membranes has not been identified. HCT is approximately 50 kDa and testing at random to find regions that insert would be inefficient. Sequence algorithms have been used to predict an HCT sequence that has the potential of being a transmembrane spanning region [89] but the insertion of this region has not been confirmed in the context of the HCT.

A method that has been useful in identifying stable regions of insertion or sites of interaction is protease protection. Liposomes should protect any regions of HCT that lie within the membrane from external protease. This would not only confirm the validity of transmembrane predictions but produce fewer regions to test. Similar studies have been effective with diphtheria toxin [90, 91] in determining regions that lie within the membrane during insertion.

In this chapter, we show that the association of LC-HCT with liposomes results in the pepsin protection of a 12 kDa and 5 kDa fragment. The two major peptides identified from these fragments map to the C-terminal region of HCT (residues 805-837). Using

the environment-sensitive fluorophore NBD, we have shown that the protected C-terminal region shifts to a more non-polar environment upon liposome association.

Methods

Protection of LC-HCT by Liposome. 50 µl of 5 mg/ml pepsin in 10 mM HCl pH 2.2 was added to 10 µl of soluble LC-HCT (10 mg/ml) or LC-HCT proteoliposomes and incubated at 37^{o}C for 12 minutes. Pepsin was quenched by the addition of loading dye (soluble LC-HCT) or 1 ml 20 mM NaAcetate pH 4.4, 100 mM NaCl (LC-HCT proteoliposomes). The proteoliposome sample was washed 3 times with 20 mM NaAcetate pH 4.4, 100 mM NaCl to remove pepsin.

Peptide Identification by Mass Spectrometry. Isolated proteoliposomes after pepsin treatment were resuspended in 20 µl of SDS-PAGE loading buffer and 2 µl of 10% SDS. Resuspended proteoliposomes were run on a NuPAGE 10% Bis-Tris-HCl precast gel. Peptide bands were excised, trypsin digested, and extracted as described [92]. Digested protein samples were desalted using Michron CapTrap desalting cartridges (Michron Bioresources) using 2% acetonitrile/0.1% TFA and eluted in a volume of 50 µl using 95% acetonitrile/0.1% TFA. The eluate was frozen on dry ice and lyophilized. Dried samples were then resuspended in 15 µl of 0.5% acetic acid in mass spectrometry-grade water. Samples were loaded onto 100 µm (internal diameter) fused silica columns packed with 12 cm of reverse phase resin (Synergi 4u Hydro RP80a, Phenomenex) and equilibrated using buffer A (0.1% TFA/5% acetonitrile). Peptides were eluted using a 120-min linear gradient from 0-80% buffer B (0.1% formic acid/80% acetonitrile) at a

flow rate of 500 nl/min. Eluted ions were analyzed by nanoESI-LC MS/MS using a Thermo LTQ linear ion trap tandem mass spectrometer, as described [93]. All acquired MS/MS data were searched against the *C. botulinum* proteome using the SEQUEST algorithm. Search results were processed and analyzed using BIGCAT [94].

Labeling Single Cysteine Mutants with IANBD. Purification for labeling of single cysteine mutants was the same as described in Chapter 2 except 1 mM Tris-(2-carboxyethyl)phosphine was added at all steps and removed during the size exclusion purification. LC-HCT from the size-exclusion column was concentrated to 1 ml (approximately 1-5 μM) and labeled overnight at 4^{o}C with a 10-fold molar excess of *N*-((2-(iodoacetoxy)ethyl)- *N*-methyl)amino-7-nitrobenz-2-oxa- 1,3-diazole (IANBD) (Molecular Probes). Excess label was removed by passing the sample over a PD10 desalting column (G.E. Healthcare). Labeled samples were concentrated to 30 μM and the labeling efficiency was determined using $\varepsilon_{478\ nm}$ of 25000 M-1cm-1 for IANBD and the $\varepsilon_{280\ nm}$ of 103280 M -1cm-1 for the LC-HCT protein. Samples not used immediately were flash frozen in liquid nitrogen and stored at -80^{o}C.

Fluorescence Spectroscopy. All fluorescence measurements were taken using a Horiba Jobin Yvon Fluoromax-3 (Horiba Scientific). The excitation wavelength for all measurements was 470 nm with a 4 nm slit width. Emission scans for both soluble and proteoliposome samples were taken from 500 nm to 600 nm in 1 nm intervals using a 4 nm slit width. A buffer background emission scan was taken by adding 246 μl 20 mM NaActetate pH 4.4, 100 mM NaCl to a round quartz cuvette (model 1924 micro cell Horiba). 4 μl of 30 μM NBD-labeled LC-HCT was added and mixed by inversion 5 times and scanned again. The maximum fluorescence intensity at 530 nm was defined as Fsol.

Proteoliposome LC-HCT spectra were taken by adding 204 µl 20 mM NaAcetate pH 4.4, 100 mM NaCl and 42 µl liposomes to a round quartz cuvette and taking an emission scan for the background. 4 µl of 30 µM NBD-labeled LC-HCT was added and mixed by inversion 5 times. The maximum fluorescence intensity at 530 nm for this sample was defined as Fmem.

Results and Discussion

Identification of protease protected fragments within BoNT/A LC-HCT proteoliposomes.

Soluble LC-HCT and LC-HCT proteoliposomes were treated with 5 mg/ml pepsin in 10 mM HCl pH 2.2. Pepsin completely proteolyzed soluble LC-HCT, but two low molecular weight bands were observed when LC-HCT was proteolyzed in the context of proteoliposomes (Figure 12A). These bands appeared to be approximately 5 kDa and 12 kDa in size. Both bands were subjected to in-gel tryptic digest and mass spectrometry analysis. Recovered tryptic peptides were separated by reversed-phase chromatography and analyzed by ESI mass spectrometry. The majority of the peptides mapped to the C-terminus of the HCT (805-820, 826-835) and localized within one region of the LC-HCT structure (Figure 12B). Both bands contained the same array of peptides and it was observed that extended treatment with pepsin resulted in a decrease of the 12 kDa band and an increase in the 5 kDa band. The 5 kDa band might represent a minimized protected region and would correspond to ~ 30 amino acids. 30 amino acids are enough to span a membrane in an α-helical or extended conformation.

A

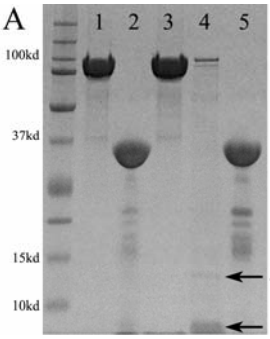

B

Band	Peptides	Count
A	826-R_GTLIGQVDR_L	38
	805-K_RLEDFDASLKDALLK_Y	23
	860-R_LLSTFTEYIK_N	9
	771-K_LESINK_A	7
	730-K_MKEALENQAEATK_A	7
B	805-K_RLEDFDASLKDALLK_Y	11
	700-K_RNEKWDEVYK_Y	8
	719-K_VNTQIDLIR_K	6
	319-K_YLLSEDTSGK_F	5

Figure 12. Liposomes protect LC-HCT peptides from pepsin cleavage. A) 20 μg of soluble LC-HCT without and with pepsin (lanes 1 and 2, respectively). 40 μg LC-HCT in proteoliposomes (lane 3) and 100 μg LC-HCT in proteoliposomes treated with pepsin (Lane 4). 8 μg of pepsin (lane 5). Arrows indicate LC-HCT peptides protected by the liposome. B) An in-gel tryptic digest of bands A and B followed by mass spectrometry suggests sequences that were protected from protease degradation in the context of the proteoliposome. The two most abundant peptides (green) overlap to one region of the LC-HCT primary sequence: 805-821 and 826-836.

Besides the peptides that mapped to the C-terminus of HCT, a few other peptides in the 5 kDa band are of interest. Another pair of peptides that appear to be a continuous region between 700-730 lies at the N-terminus of the first long helix. The 805-827 region lies antiparallel to the 700-730 region and interact with one another through hydrophobic residues. A third peptide identified was from the catalytic domain (residues 319-330). This peptide, like the 805 and 700 peptides, lies on the same face of the LC-HCT soluble structure. These peptides might suggest a face of the protein that can interact with membranes during insertion.

Steady-state fluorescence of NBD-labeled LC-HCT in soluble vs proteoliposome forms.

Based on the protease protection results alone, it is not possible to determine the nature of the protection. The protected region could be protected by the liposome as a result of insertion. It is also possible that the region has repacked in a way that it is now more resistant to pepsin. We used the environment-sensitive fluorescent dye NBD to determine how LC-HCT is protected. The emission properties of the NBD fluorophore are sensitive to the polarity of the local environment: as the dye moves from an aqueous to a nonaqueous environment, the fluorescence intensity increases and the wavelength of maximum emission intensity decreases (blue shift). Therefore, when introduced as a site-specific label, NBD can be used to differentiate between residues that are in hydrophobic and hydrophilic environments.

We generated a panel of NBD-labeled proteins with a special emphasis on two regions; 659-681 is the extended hydrophobic sequence identified by previous primary

sequence analyses [89] and the 805-820, 826-835 sequences were shown to be protease resistant in the context of proteoliposomes (Figure 13). Each LC-HCT NBD mutant was examined spectroscopically for changes in NBD fluorescence intensity between soluble and liposome associated forms. Typical spectra for a residue that shows an increase in NBD fluorescence upon association with liposomes (I830C-NBD) (Figure 14A) and a residue that shows no change in environment (I684C-NBD) (Figure 14B). Changes in fluorescence intensity were analyzed by dividing the NBD fluorescence intensity of liposome associated LC-HCT (Fmem) by the NBD fluorescence intensity of the soluble LC-HCT (Fsol) at 530 nm (Figure 14C). A large value means that the side-chain has shifted into a more hydrophobic environment upon association with the liposome.

We see that residues in the 826-835 region show Fmem/Fsol values that are > 3 and map to one tip of the HCT helical axis, specifically a loop connecting two α-helices. Mutation and testing of residues from a neighboring loop did not reveal a similar increase in NBD fluorescence (Figure 14C,D). Fluorescence quenching experiments using NBD-labeled proteins indicate that many of these residues (826-830, 832, 834-835) move into a hydrophobic environment upon conversion of LC-HCT from the soluble to liposome-associated form (Figure 14C). These data are consistent with a model in which these residues are protected at the membrane upon conversion to proteoliposome. The sequence of the loop is 826-RGTLIGQVDR-835, which is notable in that it contains charged and polar amino acids. Arginines are of particular interest as these residues are often observed at protein membrane interfaces and have been implicated in voltage gating [95, 96].

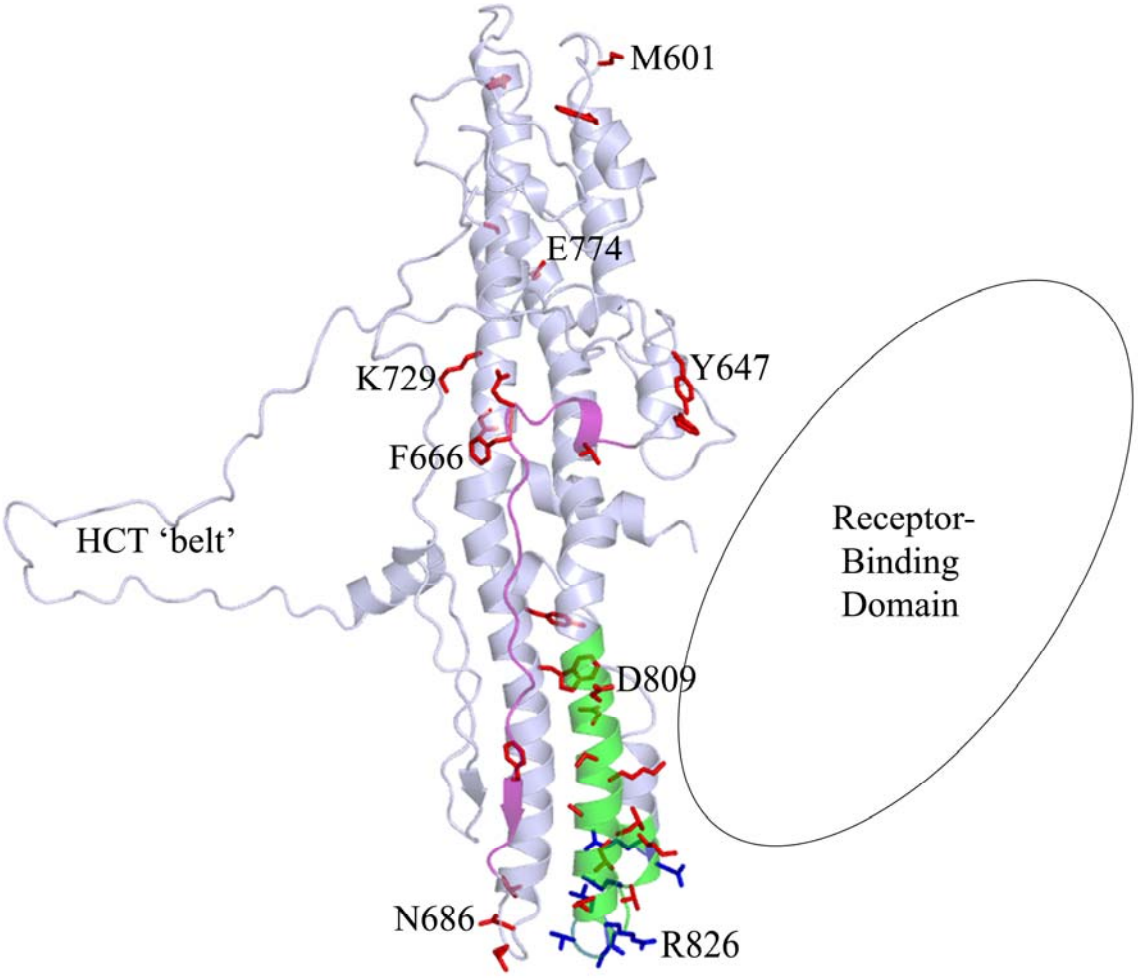

Figure 13. Locations of NBD-attached single cysteine mutants used in fluorescence studies. Residues from Fig. 14C mapped onto the structure of HCT. Residues with Fmem/Fsol > 3 are colored blue and residues with Fmem/Fsol < 3 are colored red. The peptide (805-836) identified by mass spectrometry is colored green and the predicted transmembrane sequence (659-681) is colored purple. The locations of the HCR and the HCT 'belt' that surrounds the catalytic domain are marked.

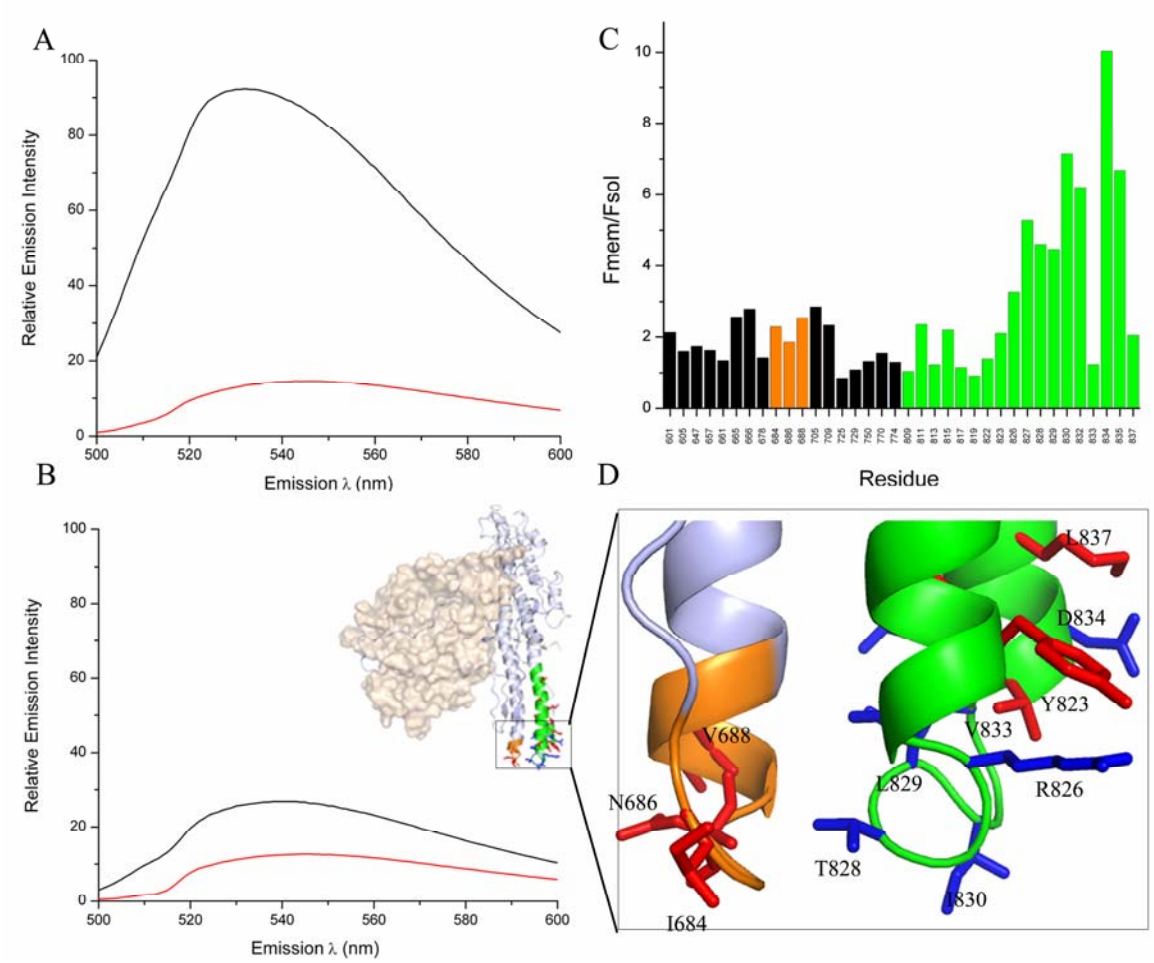

Figure 14. Fluorescence intensity of NBD attached to cysteine-substituted LC-HCT in soluble and liposome-associated forms. Emission scans of the soluble (red lines) and liposome-bound (black lines) forms of A) I830C-NBD and B) I684C-NBD at pH 4.4. The large increase in intensity and blue shift to 530 nm when I830C-NBD binds to liposomes is consistent with movement of NBD into a non-polar environment. C) Compilation of the NBD intensity changes (Fmem/Fsol) observed at 530 nm for specific LC-HCT residues when proteins in soluble (Fsol) and liposome-associated (Fmem) forms are compared. Residues were selected throughout the HCT structure with an emphasis on the protease-protected region identified in Figure 2 (805-836, green). Residues from the neighboring loop (682-688, orange) are included to show this change is specific to the protease-protected region. D) Close-up of the location of tested residues within the context of the LC-HCT structure. Residues with an Fmem/Fsol > 3 are shown in blue and residues with Fmem/Fsol < 3 are shown in red.

Summary

We describe 2 peptides that are protected from pepsin when in the presence of liposomes at low pH. These peptides correspond to one continuous amino acid stretch, 805-837, that is near the C-terminus of HCT. We used an environmentally sensitive dye, NBD, to show that this region is shifting into a more hydrophobic environment upon proteoliposome formation.

CHAPTER IV

DYNAMICS OF LC-HCT IN SOLUBLE AND LIPOSOME ASSOCIATED STATES

Introduction

Low pH and the association of BoNT with membranes are believed to introduce only minimal amounts of secondary structure changes [97]. Single domain studies have attributed the majority of those structural changes to the LC [84]. The protein translocation model would suggest that the LC would have to partially unfold in order to be passed through a channel made by the HCT We are interested in how the HCT appears to maintain its overall secondary structure with insertion into the membrane and what changes need to occur during this process.

Electron paramagnetic resonance (EPR) spectroscopy has proven to be an effective method in probing the structures of other pH-dependent pore-forming toxins [98]. In brief, the proteins are engineered to contain single cysteine residues at defined locations within the structure. The proteins are labeled with a sulfhydryl specific nitroxide reagent and inserted into model membrane liposomes. The paramagnetic resonance of the nitroxide side chain provides information on the mobility [99] and solvent accessibility of the side chain [100]. Studies of this nature have identified the α-helical transmembrane elements in colicin E1 and diphtheria toxin [101, 102].

We used EPR to investigate conformational changes and membrane insertion within the HCT. Lineshape analysis revealed that the predicted transmembrane sequence (659-681) undergoes a large conformational change. The protease protected region (805-837) shows little conformational change upon liposome association. EPR accessibility measurements, used to distinguish between polar and nonpolar environments, do not suggest a specific region is inserted into the membrane.

Methods

Labeling Single Cysteine Mutants with MTSSL. Purification for labeling of single cysteine mutants was the same as described in Chapter 2 except 1 mM DTT was added during lysis and removed on the Talon Resin. Immediately after elution from the Talon resin, 10-fold molar excess of *S*-(2,2,5,5-tetramethyl-2,5-dihydro-1H-pyrrol-3-yl)methyl methanesulfonothioate (MTSSL) dissolved in dimethylformamide was added and incubated for 4 hours at room temperature. After incubation, 5-fold molar excess of MTSSL was added and incubated overnight at 4^{o}C. Unbound MTSSL was removed during further purification.

Electron Paramagnetic Resonance of Single Cysteine Mutants. EPR spectra were collected at 23°C on a Bruker EMX spectrometer (X-band) at an incident power of 10 mW and 1.6 Gauss modulation amplitude. Spectra of soluble LC-HCT single cysteine mutants were taken at 10 mg/ml protein concentration. Proteoliposome samples were made by combining the pellets from 4 individual insertions, as described above. The combined pellets were washed 4 times with 20 mM NaAcetate pH 4.4, 100 mM NaCl

and resuspended in 40 µl of the same buffer. Power saturation experiments were carried out on a Bruker ELEXSYS spectrometer equipped with a dielectric resonator (Bruker BioSpin). Samples were loaded in gas-permeable methylpentene polymer TPX® capillaries, and the measurements were carried out under nitrogen gas alone, in the presence of 20% oxygen, or under nitrogen gas with 10 mM Nickel diaminediacetic acid (NiEDDA). The data were analyzed to obtain the parameter $P^{1/2}$ from a nonlinear least-squares fit of the power saturation curves in the program Origin (OriginLab Inc.). The EPR accessibility parameter Π was calculated as described [103]

Results and Discussion

Conformational changes in HCT structure revealed by EPR spectroscopy.

The observation that protected residues are located at one tip of the BoNT/A HCT suggests the possibility that this region merely 'dips' into the membrane without undergoing a significant structural change. To assess the extent of HCT structural change for residues throughout the structure, we collected EPR line-shape spectra for soluble and liposome associated LC-HCT using proteins labeled with MTSL at site-specific locations (Figures 15 and 16). Qualitative assessments of relative changes in side chain mobility were based on 1) the overall breadth of the spectrum along the horizontal magnetic field axis and 2) the line width of the central resonance. An increase in breadth is interpreted as a decrease in molecular ordering and/or motional frequency (24).

The 805-837 region does not appear to undergo any structural changes upon liposome association (Figure 17A). For example, L829C is a surface exposed residue in

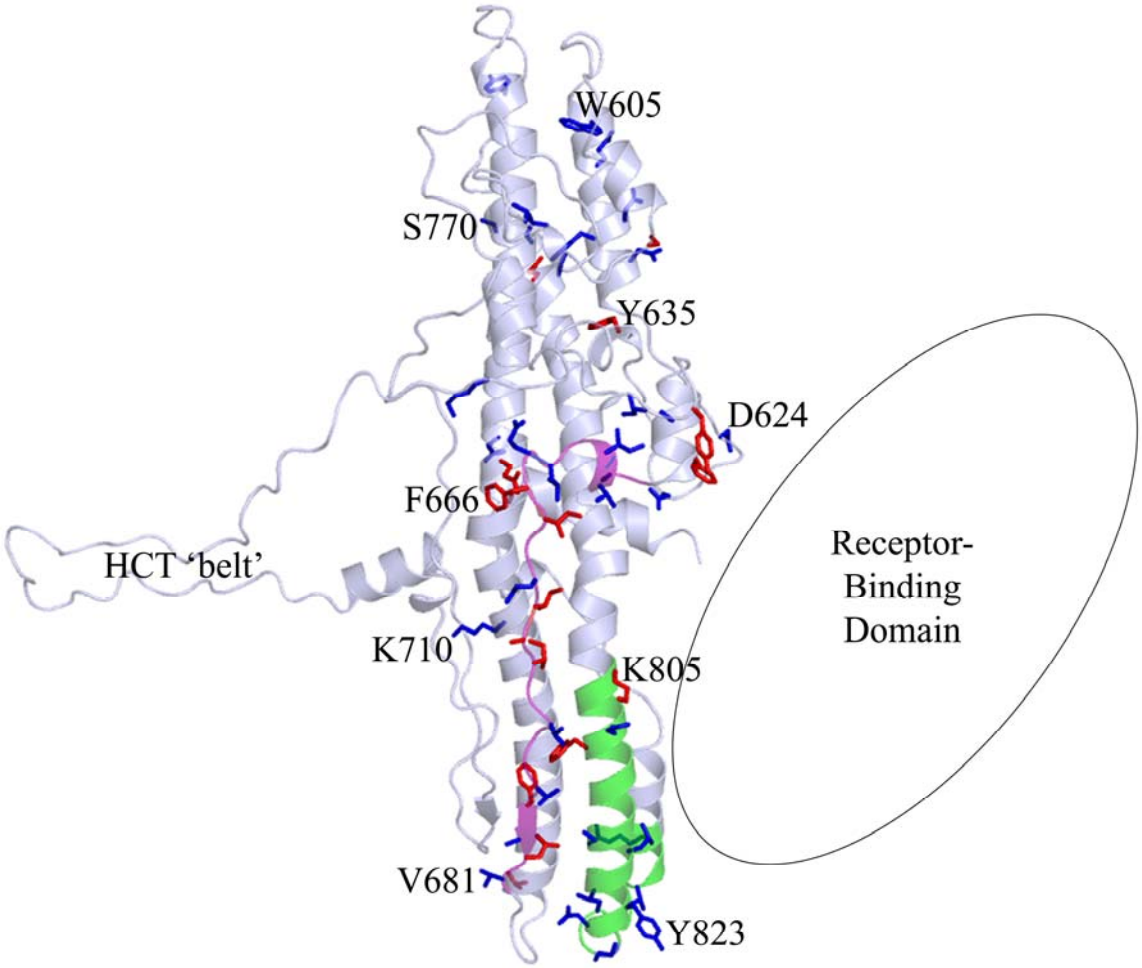

Figure 15. Locations of MTSL-attached single cysteine mutants used in lineshape analyses. Qualitative assessments of relative changes in side chain mobility were based on 1) the overall breadth of the spectrum along the horizontal magnetic field axis and 2) the line width of the central resonance. An increase or decrease in breadth is interpreted as a change in mobility and the sidechain is colored red. Side chains without significant change in lineshape are colored in blue. The peptide (805-836) identified by mass spectrometry is colored green and the predicted transmembrane sequence (659-681) is colored purple. The locations of the HCR and the HCT 'belt' that surrounds the catalytic domain are marked.

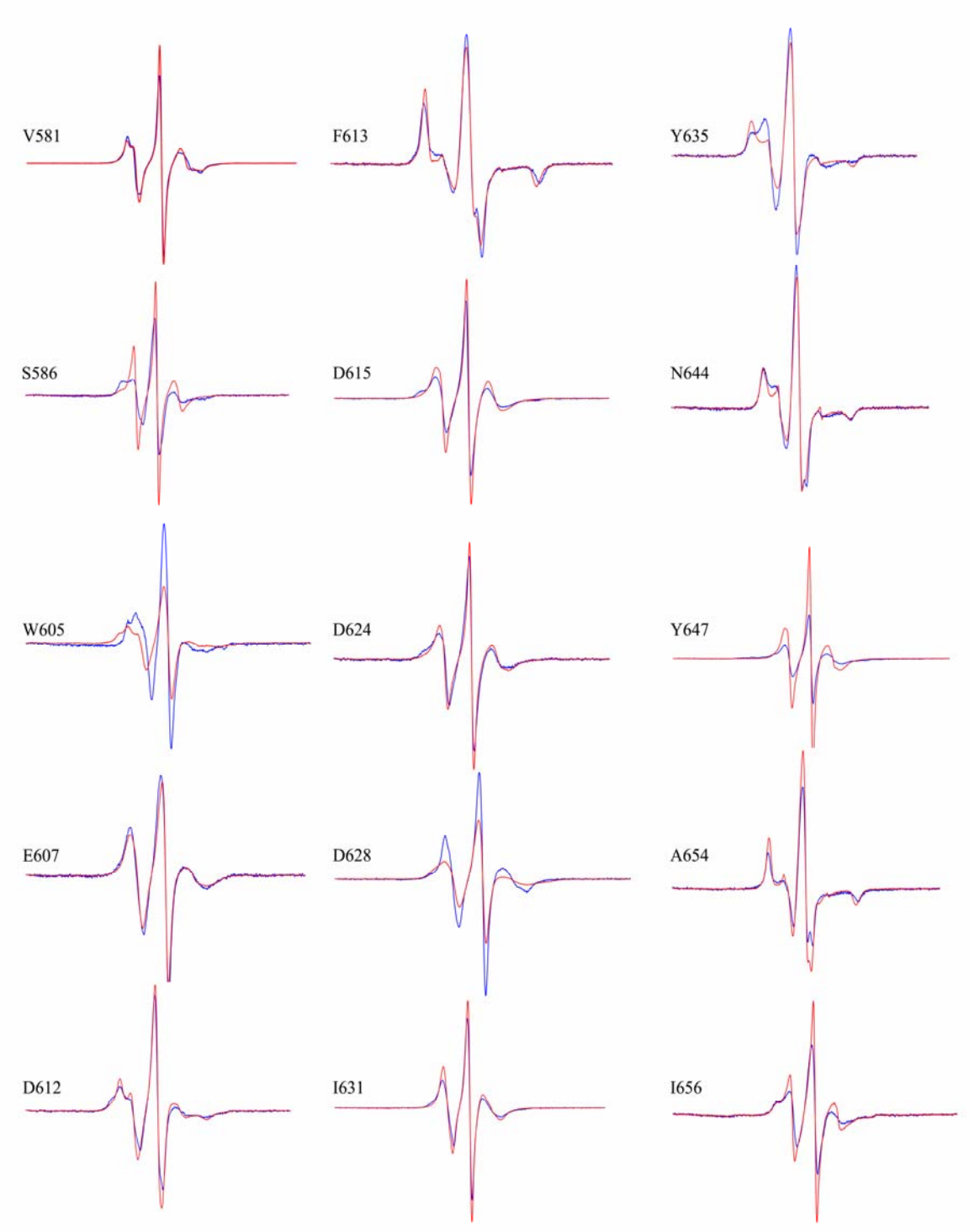
V581
F613
Y635
S586
D615
N644
W605
D624
Y647
E607
D628
A654
D612
I631
I656

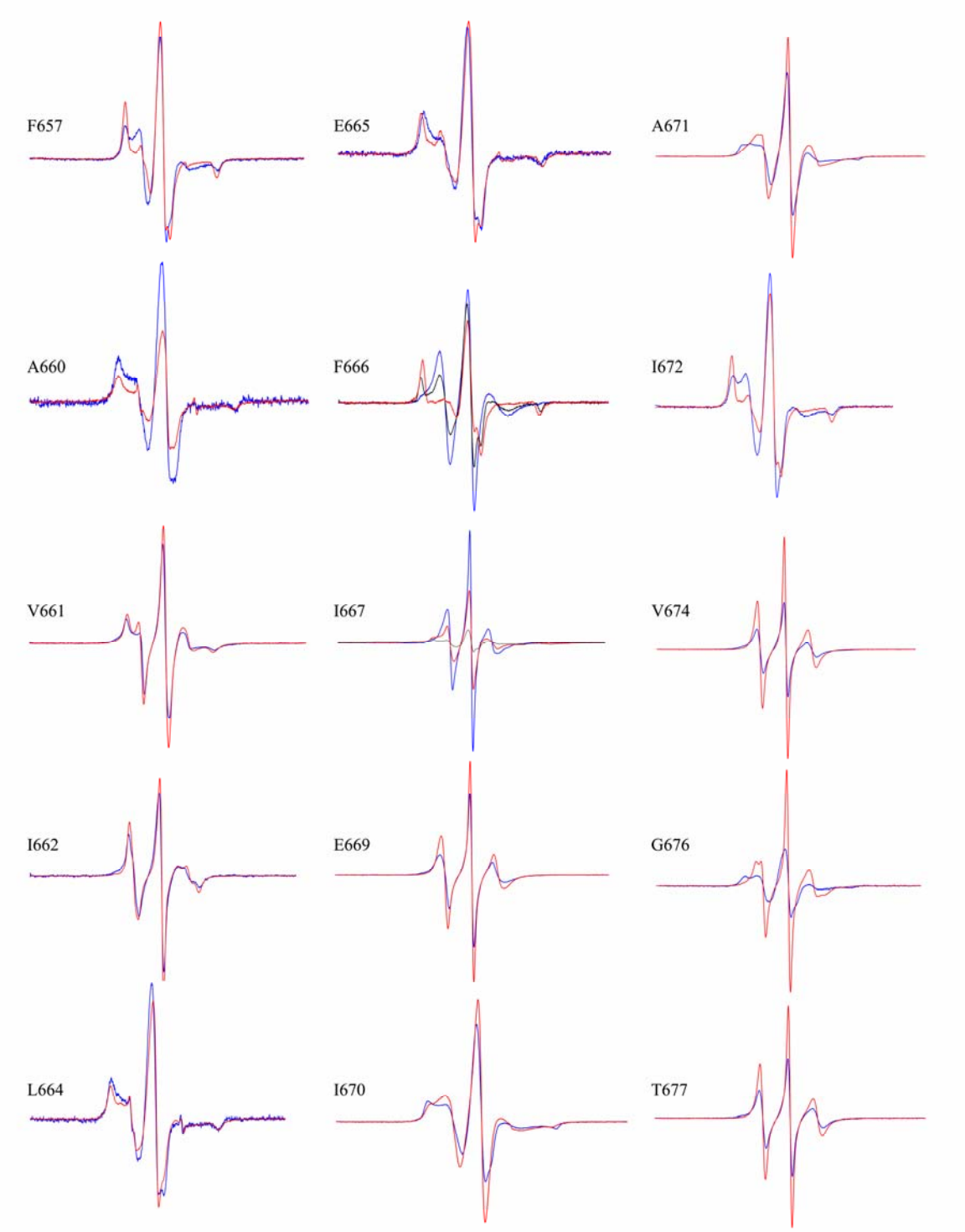
F657
E665
A671
A660
F666
I672
V661
I667
V674
I662
E669
G676
L664
I670
T677


F678
K710
S770
A679
N721
F772
L680
Q723
E774
V681
D725
S775
V688
K729
F786

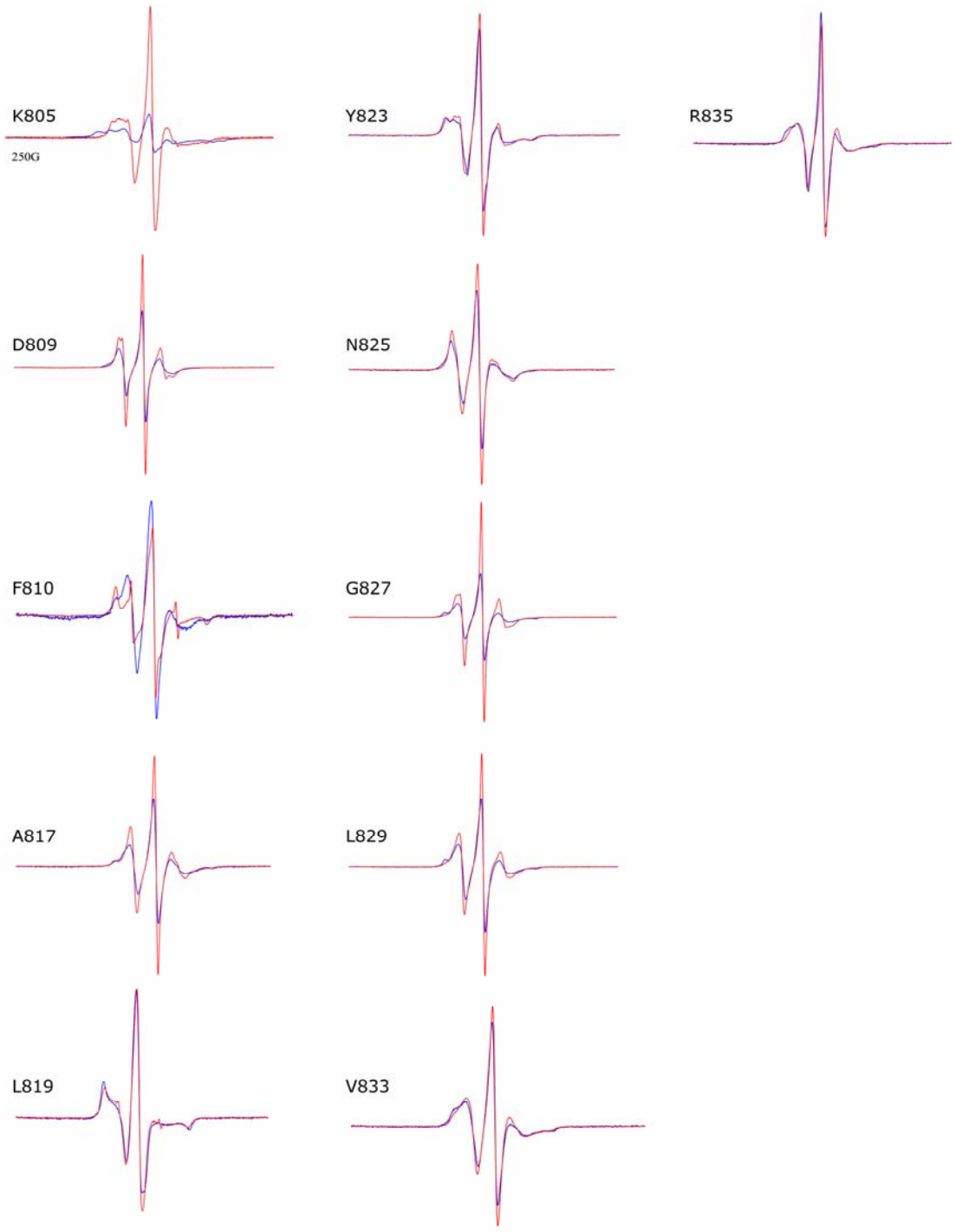

Figure 16. Lineshapes of MTSL-attached single cysteine mutants. To assess the extent of HCT structural change for residues throughout the structure, we collected EPR line-shape spectra for soluble and liposome associated LC-HCT using proteins labeled with MTSL at site-specific locations. Lineshape overlays of soluble (red) and proteoliposome pH 4.4 (blue) samples are shown. Lineshapes in black are proteoliposome samples collected at pH 5.0. All lineshapes were recorded with a 200G scan width unless otherwise specified.

the soluble form, as determined by both the structure and the EPR lineshape (Figure 17E). Upon conversion to the proteoliposome form, there is little to no change in the spectral lineshape for this residue or the nearby residues G827C and R835C. This suggests that the 826-835 loop is moving into a more hydrophobic environment as detected by NBD fluorescence but the environment shift is independent of any detectable changes in motility. Therefore it would be concluded that this loop is shifting into a new environment but without perturbations to its current structure.

While many residues tested throughout HCT showed little lineshape change upon liposome association (Figure 15), the 659-681 hydrophobic region had a large number of residues showing lineshape changes (Figure 17A). One residue, F666C, is buried at a turn within the 659-681 hydrophobic sequence and makes significant contact with the LC. The EPR lineshape analysis confirms that F666C is immobile in the protein's soluble form but is highly mobile after liposome incorporation at pH 4.4. Interestingly, the lineshape at pH 5.0 showed a mixture of mobile and immobile states, representing spectral components of F666C in the soluble and liposomes-associated forms (Figure 17B). Other residues within this region that show large lineshape changes face the hydrophobic cleft that lies between the two long helices. The lineshape change of these residues to more mobile states provides evidence that there are structural changes occurring in this region upon liposome association.

Spin-Spin interaction.

The measurement of EPR lineshapes to investigate the dynamics of BoNT association with membranes revealed a couple of residues that showed spin-spin

coupling, a phenomenon that arises when 2 spin labels are in close proximity. Spin-spin coupling is detected by lineshape broadening and the presence of peaks at low- and high-field positions not seen with a single spin label. Two residues in the HCT showed spin-spin coupling under low pH conditions. K805C showed spin-spin coupling when associated with liposomes at pH 4.4, but no spin-spin coupling was observed at pH 8.0 (Figure 17D). Residue I667C also showed spin-spin coupling but only under intermediate pH 5.0 conditions (Figure 17C), the same pH where neighboring residue F666C showed both mobile and immobile components.

The presence of spin-spin coupling in these samples suggests that the inserted protein is in an oligomeric state. This oligomerization would not be a result of receptor binding since both receptors and the HCR are missing. The presence of spin-spin at pH 5.0 for I667C, much like the presence of both mobile and immobile components in F666C, would lead us to believe that this pH might represent a transition state between the soluble and liposome-associated forms. The spin-spin measured with K805C would reflect oligomerization at a final association state within our system. We interpret these data to mean that during the process of liposome association, I667C residues from two monomers come into close proximity but as the pH decreases to 4.4 those residues separate and an oligomeric face around residue K805C is created.

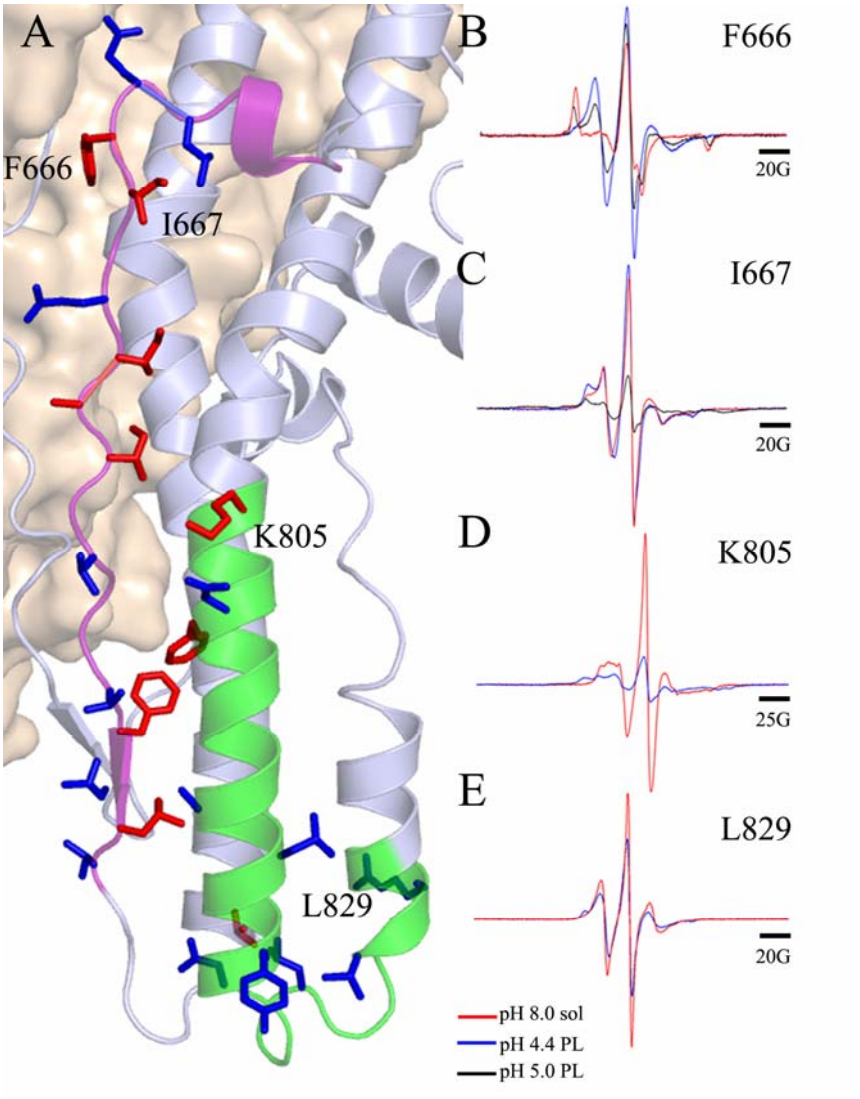

Figure 17. Lineshape measurements of MTSL attached to cysteine-substituted LC-HCT in soluble and proteoliposome forms. A) Lineshape changes in the previously described hydrophobic sequence (659-681, purple) and protease-protected region (805-836, green). Side chains are colored according to large (red) or small (blue) changes when comparing lineshapes from soluble and proteoliposome samples. Region 659-680 shows greater lineshape changes as compared to 805-836. (B-E) Representative lineshape overlays of soluble (red), proteoliposome pH 4.4 (blue), proteoliposome pH 5.0 (black) samples for mutants F666C (B), I667C (C), K805C (D) and L829C (E). A 200G scan width was used for F666C, I667C, and L829C. A 250G scan width was used for K805C. All spectra were normalized to the same number of spins.

Accessibility Measurements of MTSL-labeled mutants.

Accessibility measurements of MTSL-labeled LC-HCT mutants were conducted as a second method to differentiate between membrane inserted and solvent exposed residues in proteoliposomes. This method takes advantage of the partitioning of two paramagnetic agents, O_2 and NiEDDA. NiEDDA will remain at the highest concentration in solution and O_2 will partition into the membrane with the highest concentration found at the middle of the bilayer. The measurement of collisions between MTSL and these paramagnetic agents can indicate if the side chain is solvent exposed or membrane oriented. Analyzing the saturation behavior of the spin label can provide an accessibility parameter Π that is directly proportional to the collisions [98, 104] . Soluble and membrane associated Π values result in three categories: 1) High NiEDDA Π values suggest the residue is solvent exposed, 2) low NiEDDA Π values and low O2 Π values suggest the residue is internally packed, 3) low NiEDDA Π values and moderate/high O2 Π values suggest the residue is membrane exposed. These numbers are not absolute because other factors such as oligomerization and multiple conformations can alter residue environments, but they are a guideline.

For almost all residues tested, comparison of accessibility measurements for soluble and membrane associated LC-HCT showed a decrease in both NiEDDA and O_2 Π values (Table 2). Normally a drop in Π values is associated with individual residues or with an individual paramagnetic species, either NiEDDA or O_2. A decrease across the board means that the membrane associated sample is somehow different in how it interacts with the environment. A reason for this decrease could be due to crowding and/or oligomerization of the LC-HCT on the liposome surface.

Table 2. NiEDDA and O_2 accessibility of MTSL-labeled LC-HCT single cysteine mutants. ΔΠ values are calculated from Π(PL, proteoliposome)-Π(sol, soluble). % changes represent ΔΠ /Π(sol) x 100 and are included for those residues that show a significant change in accessibility. Most residues decrease in both O_2 and NiEDDA accessibilities when associated with liposomes. The few exceptions all have low accessibility to O_2 in both the soluble and liposome-associated forms and are, therefore, not thought to lie within the membrane.

	NiEDDA				O_2			
Residue	Π (PL)	Π (sol)	Δ Π	% change	Π (PL)	Π (sol)	Δ Π	%change
581	2.79	4.29	-1.5	-34.9	0.84	1.14	-0.30	-26.3
605	1.04	1.78	-0.74	-41.5	0.37	0.68	-0.31	-45.6
613	0.02	0.01	0.01		0.04	0.10	-0.06	
615	1.96	4.28	-2.32	-54.2	0.78	1.47	-0.69	-46.9
631	1.04	2.52	-1.48	-58.7	0.59	0.73	-0.14	-19.1
644	0.04	0.13	-0.09		0.26	0.10	0.16	
647	1.82	2.70	-0.88	-32.6	0.80	0.83	-0.03	-3.6
654	0.43	0.90	-0.53	-58.9	0.30	0.51	-0.21	-41.2
657	0.26	0.36	-0.10	-27.8	0.51	0.19	0.32	168
662	1.34	3.17	-1.83	-57.7	0.53	0.83	-0.30	-36.1
665	0.09	0.31	-0.22	-71	0.18	0.24	-0.06	-25.0
666	0.14	0.63	-0.49	-77.8	0.17	0.34	-0.17	-50.0
667	0.61	3.15	-2.54	-80.6	0.43	1.20	-0.77	-64.1
669	3.05	4.02	-0.97	-24.1	1.02	1.33	-0.31	-23.3
670	0.57	1.59	-1.02	-64.2	0.46	0.49	-0.03	-6.1
671	1.32	3.14	-1.82	-58	0.70	0.96	-0.26	-27.1
674	1.90	5.21	-3.31	-63.5	1.04	1.48	-0.44	-29.7
679	3.37	4.12	-0.75	-18.2	1.01	1.21	-0.20	-16.7
725	0.02	0.01	0.01		0.06	0.04	0.02	
750	1.55	2.21	-0.66	-29.8	0.67	0.95	-0.28	-29.5
770	0.43	1.09	-0.66	-60.6	0.29	0.43	-0.14	-32.6
774	0.81	1.66	-0.85	-51.2	0.47	0.81	-0.34	-42.0
775	0.15	0.37	-0.22	-59.5	0.21	0.27	-0.06	-22.2
817	1.50	1.95	-0.45	-23.1	0.73	1.16	-0.43	-37.1
819	0.89	2.93	-2.04	-69.6	0.48	1.04	-0.56	-53.8
823	1.35	2.46	-1.11	-45.1	0.78	1.37	-0.59	-43.1
825	1.16	3.18	-2.02	-63.5	0.70	1.26	-0.56	-44.4
827	2.34	4.21	-1.87	-44.4	1.04	1.24	-0.20	-16.1
829	0.78	3.13	-2.35	-75.1	0.94	1.03	-0.09	-8.7
833	1.14	2.81	-1.67	-59.4	0.82	1.23	-0.41	-33.3
835	1.26	3.50	-2.24	-64.0	0.84	1.46	-0.62	-42.5

F657C-MTSL and N644C-MTSL show an increase in O_2 and a decrease in NiEDDA. Normally this would suggest the residues lie within the membrane but with O_2 values this low, it could also mean that the residue is repacking in a way where solvent is being crowded out within the protein.

While the residues are not always consecutive, some trends in the data are worth noting. In the protected sequence identified in the protease protection assay, the NiEDDA accessibility seems to drop greater than the average decrease and the O_2 accessibility does not seem to drop as much as other residues. In particular L829C-MTSL shows a 75% decrease in NiEDDA when associated with liposomes but a less than 10% decrease in O_2. Most residues tested in this region show NiEDDA Π values just above 1 but higher than average O_2 values. As described in Chapter 3, this region had the highest Fmem/Fsol values of all tested mutants suggesting that it moved into a more hydrophobic environment. One would therefore expect the NiEDDA values to be minimal. This apparent discrepancy can be attributed to differences in the NBD quenching and EPR accessibility measurements.

Accessibility measurements versus NBD fluorescence.

There are several possible explanations for why the accessibility measurements do not agree with the results obtained by protease protection and fluorescence quenching. The first is that any heterogeneity resulting from inefficient incorporation into the membrane will result in a mixed population of probe environments. The assays differ significantly in how a mixed population of states would be sampled; the NBD signal is likely to be dominated by residues shifting to a nonpolar environment while the EPR

signal is likely to be dominated by residues that are not inserted in the membrane. Secondly, if BoNT forms an oligomeric structure as it inserts, the interpretation of our accessibility values could become significantly more complicated. The possibility of oligomerization in this system is supported by the observation of spin-spin coupling in the I667C and K805C samples. Thirdly, it is possible that defined transmembrane structural elements do not exist, either in nature and/or in the conditions of our proteoliposomes. In electrophysiological measurements, the channel conductivity of BoNT requires a potential gradient, a difficult thing to implement and maintain in a liposome based system. Despite the success in using EPR to analyze the transmembrane states of diphtheria toxin, many biophysical studies point to the role of multiple insertion states, shallow and deep, as diphtheria toxin enters the membrane [105, 106]. With this in mind, the 825-837 region identified here by protease protection and NBD-fluorescence studies could represent a shallow insertion of the toxin.

Docking of BoNT to membranes.

We propose that the 825-837 region mediates an initial 'docking' interaction and/or shallow insertion into the membrane and that the presence of spin-spin coupling at residues I667 and K805 suggests that these residues represent part of an oligomerization interface (Figure 18). To build a docking model for BoNT holotoxin, we also need to consider the position of the BoNT HCR. Multiple biochemical studies have highlighted the importance of ganglioside binding to the interaction of BoNT with the neuronal membrane [46] and a crystal structure of the G_{T1b} ganglioside head group bound to BoNT/A HCR is known [107]. Using the crystal structure of BoNT/A holotoxin in its

soluble state, it is difficult to envision a membrane plane that would accommodate the ganglioside-binding site at W1265 and the 825-837 loop. Furthermore, the HCR position could occlude the formation of an oligomeric structure wherein I667C and K805C molecules would be capable of spin-spin coupling. In contrast, the position of the HCR in the crystal structure of BoNT/E is in a notably different position [28]. The ganglioside-binding pocket in this structure would align easily into a membrane plane that accommodated the 825-837 loop. Furthermore, the structure can easily accommodate an oligomeric structure in which residues along the central helical axis can interact.

Summary

We did extensive EPR analysis of sites within the protected region (805-837), the predicted transmembrane region (659-681), and throughout the HCT to assess the structural changes associated with BoNT insertion to form proteoliposomes. The protected region showed no structural changes when going from the soluble to the liposome associated state. The majority of the sites tested throughout HCT showed little to no change as well. The 659-681 region was highly dynamic when transitioning between soluble and liposome associated forms. We identified two residues, I667 and K805, that show spin-spin interaction at low pH in the presence of liposomes, possibly representing an oligomeric face. These data and the crystal structures of BoNT/A and BoNT/E have allowed us to propose an initial model for how BoNT associates with liposomes at low pH.

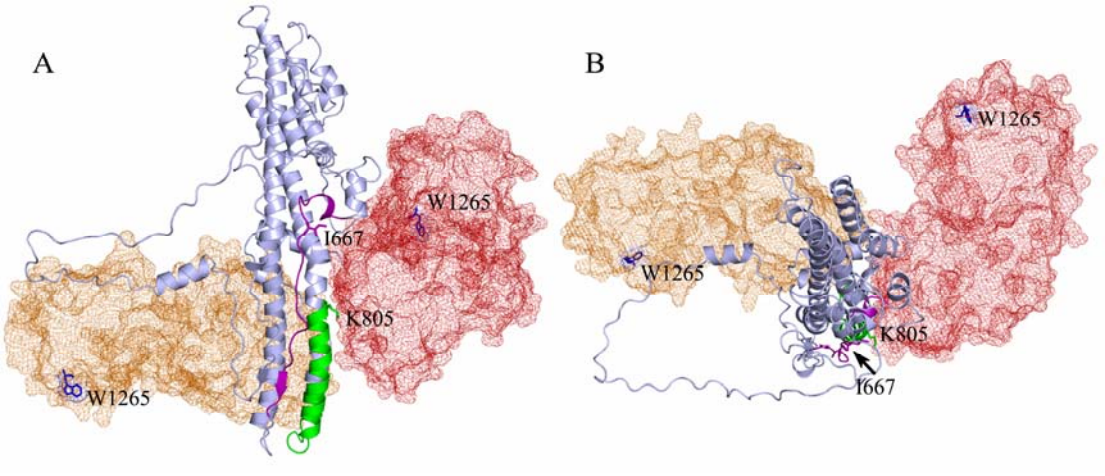

Figure 18. Model of membrane orientation based on BoNT/A and BoNT/E receptor binding domain (HCR) positions. A) In this view, the HCR of BoNT/A (red) is positioned to the right of the HCT (light blue) with the ganglioside binding W1265 residue positioned in the 'back' of the molecule. The HCR in BoNT/E (orange) is positioned such that the W1265 and 825-830 loop (green) could be located in a single plane. B) A top view of the HCT that highlights the position of the HCR from the BoNT/A (red) and BoNT/E (orange) structures. The HCR position in the BoNT/E structure would accommodate an oligomerization model that includes the spin-spin coupling observed with I667C-MTSL and K805C-MTSL.

CHAPTER V

CONCLUSIONS

Summary

Botulinum neurotoxin is the most potent toxin currently known. The majority of the structural and experimental studies related to its mechanism of action have focused on its enzymatic and receptor-binding properties. Pore formation has been studied using single channel and lipid bilayer techniques to establish that the pore is a cationic selective channel, the HCT is responsible for channel activity, and it is able to translocate the LC through the channel. Unfortunately, like many pore-forming toxins, the details of how this process occurs are missing, mainly due to the inherent difficulty in studying membrane proteins.

Chapter II describes the characterization of a recombinant BoNT/A protein, LC-HCT. LC-HCT expresses as a soluble protein that can be 'activated' with trypsin to separate the domains which are tethered by a disulfide. LC-HCT produces similar channel activity as holotoxin and can translocate the LC under low pH conditions. Unlike holotoxin, it has channel activity at neutral pH, although LC translocation does not occur. It is able to be endocytosed and cleave endogenous SNAP25 when placed directly onto Neuro2A cells despite the absence of the HCR.

LC-HCT can be reconstituted to form proteoliposomes when added to anionic liposomes in low pH conditions. This results in an irreversible binding to the liposomes that can be visualized by negative stain EM.

Chapter III describes the characterization of a C-terminal region protected from proteases when associated with liposomes. The treatment of proteoliposomes with pepsin results in 2 distinct bands on an SDS-PAGE gel that are protected from pepsin. Mass spectrometry analysis of these bands reveals common peptides that map to the C-terminal region of the HCT between residues K805-R837. Labeling of this region with NBD, an environment sensitive dye, reveals that the loop R826-L837 shifts into a hydrophobic environment upon proteoliposome formation. This could mean it is inserting into the membrane or repacking into a more hydrophobic protein environment. The region predicted to be a transmembrane helix, G659-V681, does not show this shift to a more hydrophobic environment.

Chapter IV describes the use of EPR to understand structural changes that occur during membrane association. EPR lineshapes of residues in the R826-L837 loop show little change in lineshape when soluble and membrane bound protein are compared. This revealed that the shift to a hydrophobic environment observed with NBD was not a result of local conformational changes. The region composed of G659-V681 showed large lineshape changes upon membrane association, consistent with local structural changes in this region. Lineshape analysis also revealed residues I667 and K805 show spin-spin interactions upon membrane association at pH 5 and pH 4.5, respectively. Spin-spin interaction with K805 provides evidence for an oligomeric assembly of LC-HCT upon membrane association. Spin-spin interaction of I667 disappears at pH 4.5 but its presence at pH 5.0 suggests an intermediate oligomeric form.

Accessibility measurements were used to probe the environment of the spin label to determine if the residues being tested lie within the membrane. Mutants in LC-HCT

generally showed a decrease in accessibility to both NiEDDA and O_2 when associated with liposomes, consistent with the crowding of solvent. Only N644 and F657 showed an increase in O_2 accessibility and a decrease in NiEDDA accessibility, although the magnitudes of the changes were very low. The general decrease in accessibility to NiEDDA and O_2 suggests that LC-HCT in proteoliposomes may be a heterogeneous sample thus making accessibility measurements very difficult to interpret.

Future Directions

Further Characterization of the Protected Peptides

The protected peptides described in Chapter III have provided a framework for understanding how BoNT interacts with membranes. The NBD data suggest the most abundant protected peptide, 805-837, associated the peptide lies within the bilayer. We can determine if the peptide lies within the membrane by using spin-labeled lipids as short distance quenchers of the NBD fluorescence increase. The incorporation of doxyl containing lipids into the liposomes should allow us to identify NBD-labeled residues that lie within the membrane. Incorporating the doxyl-group at different positions within the hydrocarbon chain should provide depth information. This method has been utilized when determining the membrane spanning domain for perfringolysin O [76].

Another interesting aspect of the 805-837 peptide is the number of charged amino acids. Positive amino acids within transmembrane spanning regions can define the orientation for insertion by making interactions with the lipid headgroups. In channels such as the potassium channel, they can serve as voltage gates. It would be interesting to

understand what roll, if any, these positive amino acids play in transmembrane insertion and voltage gating [95, 96]. The NBD data show that residue R826, which lies in the loop region of the protected peptide, has a remarkable increase in fluorescence upon association with the liposomes. Mutants of arginines and lysines within 805-837 could be tested by single channel patch clamp to see how they deviate from the wildtype channels in channel formation, gating, and channel conductance.

There were 3 other protected peptides that were identified by mass spectrometry from the 5 kDa band (Figure 12). One peptide 319-KYLLSEDTSGKF is within the LC and 700-KRNEKWDEVYKY and 719- KVNTQIDLIRK are in the HCT. It would be interesting to understand why both the 319 and 700 region peptides are protected and what roll they play in membrane association or translocation (Figure 19). The 700 and 719 peptides are a continuous region that lies adjacent to and makes hydrophobic contacts with the 805-826 region. These hydrophobic contacts are capped on the top by the 659 region that shows movement upon membrane association. This region has sequence similarity to a region in diphtheria toxin that is known to interact with the catalytic domain during translocation [108]. NBD studies through this region would be useful in determining if it is making contacts with the membrane. Although the 319 peptide is not involved in pore formation it seems reasonable that some of the LC would contact the membrane during the membrane binding and translocation. Any details on the LC from NBD measurements would help in building a more clear association model.

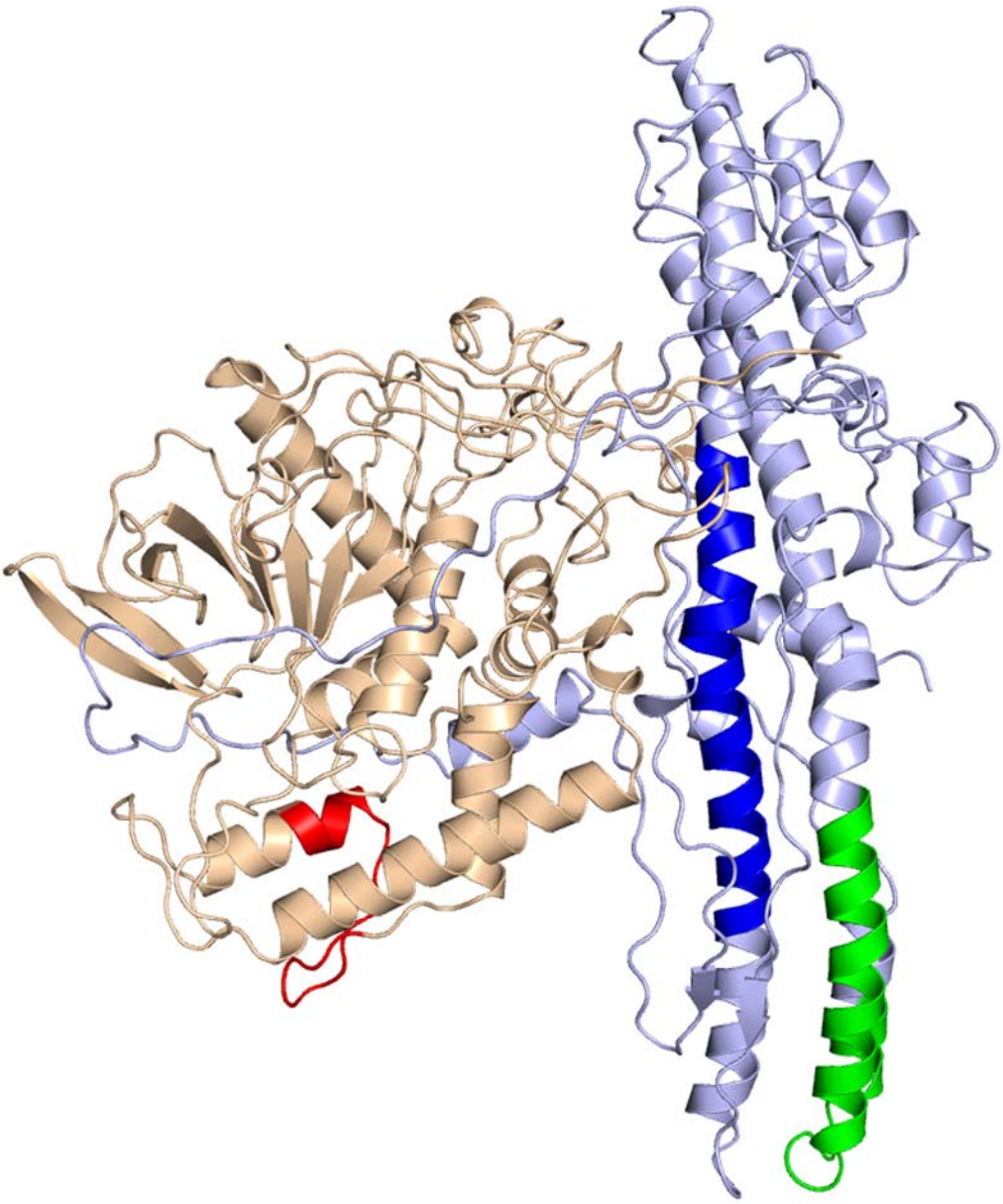

Figure 19. Locations of 3 major peptides from 5 kDa band. The 805 peptide (green) was the focus of Chapters III and IV. The 700 (dark blue) and 319 (red) peptides also showed enrichment in the 5 kDa protected band. Further analysis of these peptides by NBD fluorescence and EPR might give insight into how LC-HCT interacts with membranes.

Oligomerization of BoNT

Oligomerization is an important mechanistic aspect of pore-forming toxins such as anthrax toxin [109, 110]. Crystallization and electron microscopy have been the main techniques in determining the oligomerization state of pore forming toxins. Unfortunately BoNT has all but eluded the determination if it has an oligomeric pore state. One electron crystallography study has suggested that BoNT is capable of forming tetramers but no further work has been able to provide any evidence to support or refute this[111].

The spin-spin interactions of residues 667 and 805 presented in Chapter IV give a second glimpse into the oligomeric state of BoNT upon membrane association. LC-HCT is purified as a monomer, but upon liposome association, the spin-spin coupling suggests that at least 2 monomers are coming into close proximity. The spin interactions can be titrated by mixing labeled and unlabeled LC-HCT. Titration would result in loss of spin interaction until full signal is returned, and should allow one to assess the oligomeric state of the protein. A potential problem with this method is that spin-spin interaction requires high labeling efficiency usually greater than 95%. Lower labeling efficiency may remove signs of the spin-spin interaction or distort the oligomerization estimate since the oligomer would be a mixture of labeled and unlabeled protein prior to titration.

Gel filtration or Blue Native Page would be two similar methods at determining the oligomeric state. Both gel filtration and Blue Native can be used to determine the size of complexes. Currently the issue that has hampered these efforts from going forward is solublizing LC-HCT that has been associated with liposomes. The liposome itself is very large, variable in size, and is effectively treated as a precipitate once LC-

HCT has been associated. Prior to employing these methods, we will need to find a way of solublizing the BoNT from the liposome in a way that does not disturb the complex. This would require detergent screening in order to find a detergent that would support the same structure found in liposomes. It will also be important to see if we can repeat the line-shape and NBD measurements going directly into detergent micelles. The measurements we have from liposomes would provide a baseline for what line-shape or fluorescence changes we should see and would allow us to decide if the detergent is supporting similar structural changes in LC-HCT.

Crystallization of LC-HCT in the Membrane Associated State

X-Ray crystallography is a powerful method that would allow us to determine the oligomeric state of LC-HCT when associated with membranes but also provide details of the pore itself. Crystallization will require proper detergent that supports a homogeneous and stable pore structure. 2D crystallization is an alternative that could be done on a lipid monolayer. It would require LC-HCT to insert directly into the lipid layer without a pH gradient. Empirical assessment of conditions to generate 3D or 2D crystals will represent a priority for future studies aimed at generating an atomic model of pore structure.

Concluding Remarks

The future direction proposed here will build upon the method development that has occurred over the course of this study. The continued use of fluorescence and EPR assays, will not only help to refine our technique of reconstitution, but allow us to expand our knowledge of how BoNT interacts with membranes.

APPENDIX

Table 3. LC-HCT mutants defective in expression, stability, or labeling.

Mutant	Expression	Stability	MTSL Label
W42C	No	--	--
W117C	Poor	--	No
T583C	Yes	--	Poor
F584C	Yes	--	Poor
F585C	Yes	--	Poor
S587C	Yes	Precipitates upon addition of MTSL	No
D588C	Yes	50% Dimer Formation	Poor
V606C	Yes	--	Poor
T617C	Yes	--	Poor
V661C	Yes	Nearby nicking with trypsin	Yes
I662C	Yes	Nearby nicking with trypsin	Yes
E665C	Yes	Some autocleavage of LC	Yes
F666C	Yes	Some autocleavage of LC	Yes
P668C	Yes	--	No
W705C	Poor	--	Very Poor
Y709C	Yes	--	Very Poor
W716C	Very Poor	--	No

LIST OF PUBLICATIONS

Mushrush D.J., Koteiche H.A., Sammons M.A., Link A.J., McHaourab H.S., Lacy D.B., Studies of the mechanistic details of the pH-dependant association of botulinum neurotoxin with membranes. *J Biol Chem.* **2011** Jun 7. [Epub ahead of print]

Fischer A., **Mushrush D.J.,** Lacy D.B., Montal M., Botulinum neurotoxin devoid of receptor binding domain translocates active protease. *PLoS Pathog*. **2008** Dec;4(12):e1000245. Epub 2008 Dec 19.

BIBLIOGRAPHY

1. van Ermengem, E., *Classics in infectious diseases. A new anaerobic bacillus and its relation to botulism. E. van Ermengem. Originally published as "Ueber einen neuen anaeroben Bacillus und seine Beziehungen zum Botulismus" in Zeitschrift fur Hygiene und Infektionskrankheiten 26: 1-56, 1897.* Rev Infect Dis, 1979. **1**(4): p. 701-19.

2. van Ermengem, E., *Uber ein neuenanaeroben Bacillus und seine Beziehungen zum Botulismus.* Ztschr Hyg Infektkr, 1897. **26**: p. 1-56.

3. Hatheway, C.L., *Toxigenic clostridia.* Clin Microbiol Rev, 1990. **3**(1): p. 66-98.

4. Holdeman, L.V., *The ecology and natural history of Clostridium botulinum.* J Wildl Dis, 1970. **6**(4): p. 205-10.

5. Gimenez, D.F. and A.S. Ciccarelli, *Another type of Clostridium botulinum.* Zentralbl Bakteriol Orig, 1970. **215**(2): p. 221-4.

6. Peck, M.W., *Biology and genomic analysis of Clostridium botulinum.* Adv Microb Physiol, 2009. **55**: p. 183-265, 320.

7. Collins, M.D. and A.K. East, *Phylogeny and taxonomy of the food-borne pathogen Clostridium botulinum and its neurotoxins.* J Appl Microbiol, 1998. **84**(1): p. 5-17.

8. Sebaihia, M., et al., *Genome sequence of a proteolytic (Group I) Clostridium botulinum strain Hall A and comparative analysis of the clostridial genomes.* Genome Res, 2007. **17**(7): p. 1082-92.

9. Franciosa, G., J.L. Ferreira, and C.L. Hatheway, *Detection of type A, B, and E botulism neurotoxin genes in Clostridium botulinum and other Clostridium species by PCR: evidence of unexpressed type B toxin genes in type A toxigenic organisms.* J Clin Microbiol, 1994. **32**(8): p. 1911-7.

10. Franciosa, G., et al., *Evidence that plasmid-borne botulinum neurotoxin type B genes are widespread among Clostridium botulinum serotype B strains.* PLoS One, 2009. **4**(3): p. e4829.

11. Sobel, J., *Botulism.* Clin Infect Dis, 2005. **41**(8): p. 1167-73.

12. Hughes, J.M., et al., *Clinical features of types A and B food-borne botulism.* Ann Intern Med, 1981. **95**(4): p. 442-5.

13. Shapiro, R.L., C. Hatheway, and D.L. Swerdlow, *Botulism in the United States: a clinical and epidemiologic review.* Ann Intern Med, 1998. **129**(3): p. 221-8.

14. Sobel, J., et al., *Foodborne botulism in the United States, 1990-2000.* Emerg Infect Dis, 2004. **10**(9): p. 1606-11.

15. Werner, S.B., et al., *Wound botulism in California, 1951-1998: recent epidemic in heroin injectors.* Clin Infect Dis, 2000. **31**(4): p. 1018-24.

16. Passaro, D.J., et al., *Wound botulism associated with black tar heroin among injecting drug users.* Jama, 1998. **279**(11): p. 859-63.

17. Spika, J.S., et al., *Risk factors for infant botulism in the United States.* Am J Dis Child, 1989. **143**(7): p. 828-32.

18. Arnon, S.S., et al., *Honey and other environmental risk factors for infant botulism.* J Pediatr, 1979. **94**(2): p. 331-6.

19. Chia, J.K., et al., *Botulism in an adult associated with food-borne intestinal infection with Clostridium botulinum.* N Engl J Med, 1986. **315**(4): p. 239-41.

20. Fenicia, L., F. Anniballi, and P. Aureli, *Intestinal toxemia botulism in Italy, 1984-2005.* Eur J Clin Microbiol Infect Dis, 2007. **26**(6): p. 385-94.

21. Griffin, P.M., et al., *Endogenous antibody production to botulinum toxin in an adult with intestinal colonization botulism and underlying Crohn's disease.* J Infect Dis, 1997. **175**(3): p. 633-7.

22. Arnon, S.S., et al., *Botulinum Toxin as a Biological Weapon*. 2001. p. 1059-1070.

23. Park, J.-B. and L.L. Simpson, *Inhalational Poisoning by Botulinum Toxin and Inhalation Vaccination with Its Heavy-Chain Component.* Infect. Immun., 2003. **71**(3): p. 1147-1154.

24. Tsai, B., et al., *Protein disulfide isomerase acts as a redox-dependent chaperone to unfold cholera toxin.* Cell, 2001. **104**(6): p. 937-48.

25. Lacy, D.B., et al., *Crystal structure of botulinum neurotoxin type A and implications for toxicity.* Nat Struct Biol, 1998. **5**(10): p. 898-902.

26. Lacy, D.B. and R.C. Stevens, *Sequence homology and structural analysis of the clostridial neurotoxins.* J Mol Biol, 1999. **291**(5): p. 1091-104.

27. Swaminathan, S. and S. Eswaramoorthy, *Crystallization and preliminary X-ray analysis of Clostridium botulinum neurotoxin type B.* Acta Crystallogr D Biol Crystallogr, 2000. **56**(Pt 8): p. 1024-6.

28. Kumaran, D., et al., *Domain organization in Clostridium botulinum neurotoxin type E is unique: its implication in faster translocation.* J Mol Biol, 2009. **386**(1): p. 233-45.

29. Fischer, A., et al., *Botulinum neurotoxin devoid of receptor binding domain translocates active protease.* PLoS Pathog, 2008. **4**(12): p. e1000245.

30. Lacy, D.B. and R.C. Stevens, *Recombinant expression and purification of the botulinum neurotoxin type A translocation domain.* Protein Expr Purif, 1997. **11**(2): p. 195-200.

31. Evans, D.M., et al., *Botulinum neurotoxin type B. Its purification, radioiodination and interaction with rat-brain synaptosomal membranes.* Eur J Biochem, 1986. **154**(2): p. 409-16.

32. Montecucco, C., *How do tetanus and botulinum toxins bind to neuronal membranes?* Trends in Biochemical Sciences, 1986. **11**(8): p. 314-317.

33. Kamata, Y., et al., *Evidence for direct binding of Clostridium botulinum type E derivative toxin and its fragments to gangliosides and free fatty acids.* Biochem Biophys Res Commun, 1986. **140**(3): p. 1015-9.

34. Kitamura, M., M. Iwamori, and Y. Nagai, *Interaction between Clostridium botulinum neurotoxin and gangliosides.* Biochim Biophys Acta, 1980. **628**(3): p. 328-35.

35. Kozaki, S., et al., *Ganglioside GT1b as a complementary receptor component for Clostridium botulinum neurotoxins.* Microb Pathog, 1998. **25**(2): p. 91-9.

36. Rummel, A., et al., *The HCC-domain of botulinum neurotoxins A and B exhibits a singular ganglioside binding site displaying serotype specific carbohydrate interaction.* Mol Microbiol, 2004. **51**(3): p. 631-43.

37. Simpson, L.L. and M.M. Rapport, *Ganglioside inactivation of botulinum toxin.* J Neurochem, 1971. **18**(7): p. 1341-3.

38. Yowler, B.C. and C.L. Schengrund, *Botulinum neurotoxin A changes conformation upon binding to ganglioside GT1b.* Biochemistry, 2004. **43**(30): p. 9725-31.

39. Rummel, A., et al., *Botulinum neurotoxins C, E and F bind gangliosides via a conserved binding site prior to stimulation-dependent uptake with botulinum neurotoxin F utilising the three isoforms of SV2 as second receptor.* J Neurochem, 2009. **110**(6): p. 1942-54.

40. Yowler, B.C., R.D. Kensinger, and C.L. Schengrund, *Botulinum neurotoxin A activity is dependent upon the presence of specific gangliosides in neuroblastoma cells expressing synaptotagmin I.* J Biol Chem, 2002. **277**(36): p. 32815-9.

41. Sudhof, T.C. and J.E. Rothman, *Membrane fusion: grappling with SNARE and SM proteins.* Science, 2009. **323**(5913): p. 474-7.

42. Chapman, E.R., *How does synaptotagmin trigger neurotransmitter release?* Annual Review of Biochemistry, 2008. **77**: p. 615-641.

43. Nishiki, T., et al., *Binding of botulinum type B neurotoxin to Chinese hamster ovary cells transfected with rat synaptotagmin II cDNA.* Neurosci Lett, 1996. **208**(2): p. 105-8.

44. Nishiki, T., et al., *The high-affinity binding of Clostridium botulinum type B neurotoxin to synaptotagmin II associated with gangliosides GT1b/GD1a.* FEBS Lett, 1996. **378**(3): p. 253-7.

45. Nishiki, T., et al., *Identification of protein receptor for Clostridium botulinum type B neurotoxin in rat brain synaptosomes.* J Biol Chem, 1994. **269**(14): p. 10498-503.

46. Binz, T. and A. Rummel, *Cell entry strategy of clostridial neurotoxins.* J Neurochem, 2009. **109**(6): p. 1584-95.

47. Jin, R., et al., *Botulinum neurotoxin B recognizes its protein receptor with high affinity and specificity.* Nature, 2006. **444**(7122): p. 1092-5.

48. Chai, Q., et al., *Structural basis of cell surface receptor recognition by botulinum neurotoxin B.* Nature, 2006. **444**(7122): p. 1096-100.

49. Dyson, H.J. and P.E. Wright, *Intrinsically unstructured proteins and their functions.* Nat Rev Mol Cell Biol, 2005. **6**(3): p. 197-208.

50. Dong, M., et al., *Synaptotagmins I and II mediate entry of botulinum neurotoxin B into cells.* J Cell Biol, 2003. **162**(7): p. 1293-303.

51. Dong, M., et al., *SV2 is the protein receptor for botulinum neurotoxin A.* Science, 2006. **312**(5773): p. 592-6.

52. Dong, M., et al., *Glycosylated SV2A and SV2B mediate the entry of botulinum neurotoxin E into neurons.* Mol Biol Cell, 2008. **19**(12): p. 5226-37.

53. Fu, Z., et al., *Glycosylated SV2 and gangliosides as dual receptors for botulinum neurotoxin serotype F.* Biochemistry, 2009. **48**(24): p. 5631-41.

54. Peng, L., et al., *Botulinum Neurotoxin D Uses Synaptic Vesicle Protein SV2 and Gangliosides as Receptors.* PLoS Pathog, 2011. **7**(3): p. e1002008.

55. Kroken, A.R., et al., *Unique Ganglioside Binding by Botulinum Neurotoxins C and D-SA.* FEBS Journal: p. no-no.

56. Strotmeier, J., et al., *The biological activity of botulinum neurotoxin type C is dependent upon novel types of ganglioside binding sites.* Molecular Microbiology: p. no-no.

57. Schiavo, G., et al., *Identification of the nerve terminal targets of botulinum neurotoxin serotypes A, D, and E.* J Biol Chem, 1993. **268**(32): p. 23784-7.

58. Blasi, J., et al., *Botulinum neurotoxin A selectively cleaves the synaptic protein SNAP-25.* Nature, 1993. **365**(6442): p. 160-3.

59. Schiavo, G., et al., *Botulinum neurotoxins serotypes A and E cleave SNAP-25 at distinct COOH-terminal peptide bonds.* FEBS Lett, 1993. **335**(1): p. 99-103.

60. Williamson, L.C., et al., *Clostridial neurotoxins and substrate proteolysis in intact neurons: botulinum neurotoxin C acts on synaptosomal-associated protein of 25 kDa.* J Biol Chem, 1996. **271**(13): p. 7694-9.

61. Foran, P., et al., *Botulinum neurotoxin C1 cleaves both syntaxin and SNAP-25 in intact and permeabilized chromaffin cells: correlation with its blockade of catecholamine release.* Biochemistry, 1996. **35**(8): p. 2630-6.

62. Binz, T., et al., *Proteolysis of SNAP-25 by types E and A botulinal neurotoxins.* J Biol Chem, 1994. **269**(3): p. 1617-20.

63. Schiavo, G., et al., *Tetanus and botulinum-B neurotoxins block neurotransmitter release by proteolytic cleavage of synaptobrevin.* Nature, 1992. **359**(6398): p. 832-5.

64. Schiavo, G., et al., *Botulinum neurotoxin serotype F is a zinc endopeptidase specific for VAMP/synaptobrevin.* J Biol Chem, 1993. **268**(16): p. 11516-9.

65. Schiavo, G., et al., *Botulinum G neurotoxin cleaves VAMP/synaptobrevin at a single Ala-Ala peptide bond.* J Biol Chem, 1994. **269**(32): p. 20213-6.

66. Yamasaki, S., et al., *Botulinum neurotoxin type G proteolyses the Ala81-Ala82 bond of rat synaptobrevin 2.* Biochem Biophys Res Commun, 1994. **200**(2): p. 829-35.

67. Yamasaki, S., et al., *Cleavage of members of the synaptobrevin/VAMP family by types D and F botulinal neurotoxins and tetanus toxin.* J Biol Chem, 1994. **269**(17): p. 12764-72.

68. Blasi, J., et al., *Botulinum neurotoxin C1 blocks neurotransmitter release by means of cleaving HPC-1/syntaxin.* Embo J, 1993. **12**(12): p. 4821-8.

69. Schiavo, G., et al., *Botulinum neurotoxin type C cleaves a single Lys-Ala bond within the carboxyl-terminal region of syntaxins.* J Biol Chem, 1995. **270**(18): p. 10566-70.

70. Breidenbach, M.A. and A.T. Brunger, *Substrate recognition strategy for botulinum neurotoxin serotype A.* Nature, 2004. **432**(7019): p. 925-9.

71. Kumaran, D., et al., *Substrate Binding Mode and Its Implication on Drug Design for Botulinum Neurotoxin A.* PLoS Pathog, 2008. **4**(9): p. e1000165.

72. Brunger, A.T., et al., *Botulinum neurotoxin heavy chain belt as an intramolecular chaperone for the light chain.* PLoS Pathog, 2007. **3**(9): p. 1191-4.

73. Muchmore, S.W., et al., *X-ray and NMR structure of human Bcl-xL, an inhibitor of programmed cell death.* Nature, 1996. **381**(6580): p. 335-41.

74. Parker, M.W. and F. Pattus, *Rendering a membrane protein soluble in water: a common packing motif in bacterial protein toxins.* Trends Biochem Sci, 1993. **18**(10): p. 391-5.

75. Gouaux, E., *Channel-forming toxins: tales of transformation.* Curr Opin Struct Biol, 1997. **7**(4): p. 566-73.

76. Shepard, L.A., et al., *Identification of a membrane-spanning domain of the thiol-activated pore-forming toxin Clostridium perfringens perfringolysin O: an alpha-helical to beta-sheet transition identified by fluorescence spectroscopy.* Biochemistry, 1998. **37**(41): p. 14563-74.

77. Mueller, M., et al., *The structure of a cytolytic alpha-helical toxin pore reveals its assembly mechanism.* Nature, 2009. **459**(7247): p. 726-30.

78. Blaustein, R.O., et al., *The N-terminal half of the heavy chain of botulinum type A neurotoxin forms channels in planar phospholipid bilayers.* FEBS Lett, 1987. **226**(1): p. 115-20.

79. Donovan, J.J. and J.L. Middlebrook, *Ion-conducting channels produced by botulinum toxin in planar lipid membranes.* Biochemistry, 1986. **25**(10): p. 2872-6.

80. Fisher, A. and M. Montal, *Characterization of Clostridial botulinum neurotoxin channels in neuroblastoma cells.* Neurotox Res, 2006. **9**(2-3): p. 93-100.

81. Hoch, D.H., et al., *Channels formed by botulinum, tetanus, and diphtheria toxins in planar lipid bilayers: relevance to translocation of proteins across membranes.* Proc Natl Acad Sci U S A, 1985. **82**(6): p. 1692-6.

82. Sheridan, R.E., *Gating and permeability of ion channels produced by botulinum toxin types A and E in PC12 cell membranes.* Toxicon, 1998. **36**(5): p. 703-17.

83. Finkelstein, A., *Channels formed in phospholipid bilayer membranes by diphtheria, tetanus, botulinum and anthrax toxin.* J Physiol (Paris), 1990. **84**(2): p. 188-90.

84. Koriazova, L.K. and M. Montal, *Translocation of botulinum neurotoxin light chain protease through the heavy chain channel.* Nat Struct Biol, 2003. **10**(1): p. 13-8.

85. Fischer, A. and M. Montal, *Crucial role of the disulfide bridge between botulinum neurotoxin light and heavy chains in protease translocation across membranes.* J Biol Chem, 2007. **282**(40): p. 29604-11.

86. Fischer, A. and M. Montal, *Single molecule detection of intermediates during botulinum neurotoxin translocation across membranes.* Proc Natl Acad Sci U S A, 2007. **104**(25): p. 10447-52.

87. Fischer, A., et al., *Bimodal modulation of the botulinum neurotoxin protein-conducting channel.* Proc Natl Acad Sci U S A, 2009. **106**(5): p. 1330-5.

88. Fu, F.N., D.D. Busath, and B.R. Singh, *Spectroscopic analysis of low pH and lipid-induced structural changes in type A botulinum neurotoxin relevant to membrane channel formation and translocation.* Biophys Chem, 2002. **99**(1): p. 17-29.

89. Oblatt-Montal, M., et al., *Formation of ion channels in lipid bilayers by a peptide with the predicted transmembrane sequence of botulinum neurotoxin A.* Protein Sci, 1995. **4**(8): p. 1490-7.

90. Cabiaux, V., et al., *Topology of diphtheria toxin B fragment inserted in lipid vesicles.* Mol Microbiol, 1994. **11**(1): p. 43-50.

91. McGill, S., et al., *Membrane interactions of diphtheria toxin analyzed using in vitro synthesized mutants.* Embo J, 1989. **8**(10): p. 2843-8.

92. Shevchenko, A., et al., *In-gel digestion for mass spectrometric characterization of proteins and proteomes.* Nat Protoc, 2006. **1**(6): p. 2856-60.

93. Link, A.J., et al., *Purifying protein complexes for mass spectrometry: applications to protein translation.* Methods, 2005. **35**(3): p. 274-90.

94. McAfee, K.J., et al., *Analyzing proteomes and protein function using graphical comparative analysis of tandem mass spectrometry results.* Mol Cell Proteomics, 2006. **5**(8): p. 1497-513.

95. Aggarwal, S.K. and R. MacKinnon, *Contribution of the S4 segment to gating charge in the Shaker K+ channel.* Neuron, 1996. **16**(6): p. 1169-77.

96. Borjesson, S.I. and F. Elinder, *Structure, function, and modification of the voltage sensor in voltage-gated ion channels.* Cell Biochem Biophys, 2008. **52**(3): p. 149-74.

97. Singh, B.R. and B.R. DasGupta, *Structure of heavy and light chain subunits of type A botulinum neurotoxin analyzed by circular dichroism and fluorescence measurements.* Mol Cell Biochem, 1989. **85**(1): p. 67-73.

98. Oh, K.J., et al., *Site-directed spin labeling of proteins. Applications to diphtheria toxin.* Methods Mol Biol, 2000. **145**: p. 147-69.

99. McHaourab, H.S., et al., *Motion of spin-labeled side chains in T4 lysozyme. Correlation with protein structure and dynamics.* Biochemistry, 1996. **35**(24): p. 7692-704.

100. Hubbell, W.L., et al., *Watching proteins move using site-directed spin labeling.* Structure, 1996. **4**(7): p. 779-83.

101. Oh, K.J., et al., *Organization of diphtheria toxin T domain in bilayers: a site-directed spin labeling study.* Science, 1996. **273**(5276): p. 810-2.

102. Shin, Y.K., et al., *Colicin E1 binding to membranes: time-resolved studies of spin-labeled mutants.* Science, 1993. **259**(5097): p. 960-3.

103. Altenbach, C., et al., *Accessibility of nitroxide side chains: absolute Heisenberg exchange rates from power saturation EPR.* Biophys J, 2005. **89**(3): p. 2103-12.

104. Farahbakhsh, Z.T., C. Altenbach, and W.L. Hubbell, *Spin labeled cysteines as sensors for protein-lipid interaction and conformation in rhodopsin.* Photochem Photobiol, 1992. **56**(6): p. 1019-33.

105. Wang, Y., et al., *Identification of shallow and deep membrane-penetrating forms of diphtheria toxin T domain that are regulated by protein concentration and bilayer width.* J Biol Chem, 1997. **272**(40): p. 25091-8.

106. Rosconi, M.P. and E. London, *Topography of helices 5-7 in membrane-inserted diphtheria toxin T domain: identification and insertion boundaries of two hydrophobic sequences that do not form a stable transmembrane hairpin.* J Biol Chem, 2002. **277**(19): p. 16517-27.

107. Stenmark, P., et al., *Crystal structure of botulinum neurotoxin type A in complex with the cell surface co-receptor GT1b-insight into the toxin-neuron interaction.* PLoS Pathog, 2008. **4**(8): p. e1000129.

108. Ratts, R., et al., *A conserved motif in transmembrane helix 1 of diphtheria toxin mediates catalytic domain delivery to the cytosol.* Proc Natl Acad Sci U S A, 2005. **102**(43): p. 15635-40.

109. Lacy, D.B., et al., *Structure of heptameric protective antigen bound to an anthrax toxin receptor: a role for receptor in pH-dependent pore formation.* Proc Natl Acad Sci U S A, 2004. **101**(36): p. 13147-51.

110. Katayama, H., et al., *GroEL as a molecular scaffold for structural analysis of the anthrax toxin pore.* Nat Struct Mol Biol, 2008. **15**(7): p. 754-60.

111. Schmid, M.F., J.P. Robinson, and B.R. DasGupta, *Direct visualization of botulinum neurotoxin-induced channels in phospholipid vesicles.* Nature, 1993. **364**(6440): p. 827-30.